Bed and width oscillations form coherent patterns in a partially confined, regulated gravel-cobble bedded river adjusting to anthropogenic disturbances

Rocko A. Brown*[1,2] and Gregory B. Pasternack[1]

1-University of California, Davis, One Shields Avenue, Davis, CA, USA.

2-Environmental Science Associates, 2600 Capitol Avenue, Suite 200, Sacramento, CA USA

* Corresponding author. Tel.: +1 510-333-5131; E-mail: rokbrown@ucdavis.edu.

Abstract

This paper demonstrates a relatively new method of analysis for flow dependent patterns in meter-scale resolution river digital elevation models, termed geomorphic covariance structures (GCSs). A GCS is a bivariate spatial relationship amongst or between variables along a pathway in a river corridor. It is not a single metric as in statistical covariance, but a spatial series, and hence can capture spatially explicit geomorphic structure. Variables assessed can be flow-independent measures of topography (e.g., bed elevation, centerline curvature, and cross section asymmetry) and sediment size as well as flow-dependent hydraulics (e.g., top width, depth, velocity, and shear stress; Brown, 2014), topographic change, and biotic variables (e.g., biomass and habitat utilization). The GCS analysis is used to understand if and how bed elevation and flow-dependent channel top width are organized in a partially confined, incising gravel-cobbled bed river with multiple spatial scales of anthropogenic and natural landform heterogeneity across a range of discharges on 6.4 km of the lower Yuba River in California, USA. A key conclusion is that the test river exhibited positively covaring oscillations of bed elevation and channel width across all flows analyzed. These covarying oscillations were found to be quasi-periodic at channel forming flows, scaling with the length scales of pools and riffles. Thus it appears that alluvial rivers organize their topography to have quasi-periodic shallow and wide and narrow and deep cross section geometry, even despite ongoing incision.

1. Introduction

Understanding the spatial organization of river systems in light of natural and

anthropogenic change is extremely important, because it can provide information to assess, manage and restore them to ameliorate worldwide freshwater fauna declines (Frissell et al., 1986; Richter et al., 1997). Alluvial rivers found in transitional upland-lowland environments with slopes < 0.02 and median diameter bed sediments ranging from 8 to 256 mm can exhibit scale dependent organization of their bed sediments (Milne, 1982), bed elevation profile (Madej, 2001), cross section geometry (Rayberg and Neave, 2008) and morphological units (Keller and Melhorn, 1978; Thomson et al., 2001). For these rivers a plethora of studies spanning analytical, empirical and numerical domains suggest that at channel-forming flows there is a tendency for covarying bankfull bed and width undulations amongst morphologic units such as pools and riffles (Brown et al., 2016). That is, relatively wide areas have higher relative bed elevations and relatively narrow areas have lower relative bed elevations. While covarying bed and width undulations have been evaluated in field studies using cross section data (Richards, 1976a,b), in models of sediment transport and water flow (Repetto and Tubino, 2001), flume studies (Nelson et al., 2015) and in theoretical treatments (Huang et al., 2004), this idea has never been evaluated in a morphologically dynamic river corridor for which a meter-scale digital elevation model is available across a wide range of discharges, from a fraction of to orders of magnitude more than bankfull. The purpose of this paper is twofold. First, it aims to demonstrate how meter-scale resolution topography can be analyzed with hydraulic model outputs to generate flow dependent geomorphic covariance structures (GCS) of bed elevation and wetted width. We developed this new term in recent articles (Brown et al., 2014; Brown and Pasternack, 2014; Brown et al., 2016) as a result of the growing importance of

61 understanding the variability of rivers as a first-order control on their dynamics. A GCS
62 is not the statistical metric known as covariance, which summarizes the relation
63 between two series in one number, but is instead a spatial series created from the
64 product of two any detrended and standardized geomorphic variables computed or
65 measured along a pathway in a river corridor. Variables used in a GCS can be flow-
66 independent measures of topography (e.g., bed elevation, centerline curvature, and
67 cross section asymmetry) and sediment size, as well as flow-dependent hydraulics
68 (e.g., top width, depth, velocity, and shear stress; Brown, 2014), topographic change,
69 and biotic variables (e.g., biomass and habitat utilization).

70 Second, we aim to use these methods and concepts to understand if and how bed
71 elevation and flow-dependent channel width are organized in a partially confined,
72 incising, regulated gravel-cobbled bed river with multiple spatial scales of landform
73 heterogeneity across a range of discharges. The analysis of geometric organization was
74 accomplished through a suite of spatial series analyses using a 9-km reach of the lower
75 Yuba River (LYR) in California, USA as a testbed. Our central hypothesis is that the test
76 river reach will exhibit covarying and quasi-periodic bed and width oscillations, and that
77 due to river corridor heterogeneity and antecedent flow conditions these patterns may
78 be dominant in a range of channel forming flows. Knowledge of spatial patterning is
79 commonly used to infer the geomorphic processes that yielded that patterning (Davis,
80 1909; Thornbury, 1954) and/or what future processes will be driven by the current
81 spatial structure of landforms (Leopold and Maddock, 1953; Schumm, 1971; Brown and
82 Pasternack, 2014). However, such inferences rarely include transparent, objective
83 spatial analysis of topographic structure, so this study provides a new concept and

84 methodology accessible to most practitioners to substantiate the ideas behind the
85 process-morphology linkages they envision to be driven by variability in topography.
86
87 *1.1 Background*
88 A multitude of numerical, field, and theoretical studies have shown that gravel
89 bed rivers have covarying oscillations between bed elevation and channel width related
90 to riffle-pool maintenance. The joint periodicity in oscillating thalweg and bankfull width
91 series for pool-riffle sequences in gravel bed rivers was identified by Richards (1976b)
92 who noted that riffles have widths that are on average greater than those of pools, and
93 he attributed this to flow deflection over riffles into the channel banks. Since then, many
94 studies related to processes that rejuvenate or maintain the relief between bars and
95 pools (i.e., “maintenance” or “self-maintenance”) have implied a specific spatial
96 correlation of width and depth between the pool and riffle at the bankfull or channel
97 forming discharge (Wilkinson et al. 2004; MacWilliams et al., 2006; Caamano et al.,
98 2009; Thompson, 2010). For example, Caamano et al. (2009) derived a criterion for the
99 occurrence of a mean reversal in velocity (Keller, 1971) that implies a specific
100 correlation of the channel geometry of alluvial channels with undulating bed profiles.
101 Specifically, for a reversal in mean velocity at the bankfull or channel forming discharge
102 (holding substrate composition constant), the riffle must be wider than the pool and the
103 width variation should be greater than the depth variation between the riffle and residual
104 pool depth. Milan et al. (2001) evaluated several riffle-pool couplets, from a base flow
105 to just over the bankfull discharge. They found that convergence and reversals in
106 section-averaged velocity and shear stress were complex and non-uniform, which

107 suggests that different morphologic units may be maintained at different discharges.
108 Wilkinson et al. (2004) explicitly showed that phase shifts in shear stress from the riffle
109 to the pool between high and low discharge required positively covarying bed and width
110 undulations. White et al. (2010) showed how valley width oscillations influence riffle
111 persistence despite larger channel altering floods and interdecadal valley incision.
112 Sawyer et al (2010) used two-dimensional (2D) hydrodynamic modeling and digital
113 elevation model (DEM) differencing to illustrate how variations in wetted width and bed
114 elevation can modulate regions of peak velocity and channel change at a pool-riffle-run
115 sequence across a range of discharges from 0.15 to 7.6 times bankfull discharge.
116 DeAlmeida and Rodriguez (2012) used a 1D morphodynamic model to explore the
117 evolution of riffle-pool bedforms from an initially flat bed, while maintaining the channel
118 width variability. The resulting simulations had close agreement to the actual bed profile
119 in their model. Thus, their study is another example that channel width can exert
120 controls on the structure of the bed profile. The flows at which the above processes are
121 modulated vary in the literature.
122 From a system perspective, bed and width undulations, both jointly and in
123 isolation, are a means of self-adjustment in alluvial channels that minimize the time rate
124 of potential energy expenditure per unit mass of water in accordance with the law of
125 least time rate of energy expenditure (Langbein and Leopold, 1962; Yang, 1971;
126 Cherkauer, 1973; Wohl et al., 1999). For bed profiles, Yang (1971) and Cherkauer
127 (1973) showed that undulating bed relief is a preferred configuration of alluvial channels
128 that minimize the time rate of potential energy expenditure. Using field, flume, and
129 numerical methods Wohl et al. (1999) showed that valley wall oscillations also act to

regulate flow energy analogous to bedforms. In analyzing reach scale energy constraints on river behavior Huang et al. (2004) quantitatively showed that wide/shallow sections and deep/narrow sections are two end member cross sectional configurations necessary for efficiently expending excess energy for rivers, so these two types of cross sections imply covarying bed and width undulations as a means of expending excess energy. Therefore the above studies suggest that both bed and width oscillations are a means to optimize channel geometry for the dissipation of excess flow energy. The question now is the extent to which this well-developed theory plays out in real rivers, especially now that meter-scale river DEMs are available.

Flows that drive channel maintenance in Western U.S. rivers, such as the test river in this study (described in detail in Section 3 below), are thought to typically have annual recurrence intervals ranging from 1.2 to 5 years (Williams,1978; Andrews, 1980; Nolan et al., 1987). Most of the literature investigating riffle-pool maintenance discussed above report bedform sustaining flow reversals occurring at or near bankfull, often with no specificity to the frequency of these events (Lisle, 1979; Wilkinson et al., 2004). Studies that do report recurrence intervals have ranged from the 1.2 to 7.7 year recurrence flows (Keller, 1971; Sawyer et al., 2010). However, many rivers exhibit multiple scales of freely formed and forced landscape heterogeneity that should influence fluvial geomorphology when the flow interacts with them, no matter the magnitude (Church, 2006; Gangodagamage et al., 2007). For example, Strom and Pasternack (2016) showed that the geomorphic setting can influence the stage at which reversals in peak velocity occur. In their study an unconfined anastomizing reach experienced velocity reversals at flows ranging from 1.5 to 2.5 year recurrence flows,

compared to 2.5 to 4.7 year recurrence flows for a valley-confined reach. Given that river geometry can record memory from past floods (Yu and Wolman, 1987), and the presence of multiple layers of topographic variability (Brown and Pasternack, 2014), it is hypothesized that covarying bed and width undulations could also be present at discharges other than bankfull.

1.2 Study Objectives

This study sought to evaluate the longitudinal geomorphic covariance structure of bed elevation and flow-dependent width undulations in a river valley for a wide range of discharges above and below the bankfull discharge– a breadth never evaluated before. The primary goal of this study was to determine if there are covarying bed and width oscillations in an incising gravel/cobble river, if they exhibit any periodicity, and how they vary with discharge. Based on the literature review above, the expectation is that a quasi-oscillatory positive GCSs should exist, with the strongest relationship occurring for a broad range of channel forming flows. A secondary objective is to demonstrate how geomorphic covariance structures for bed and wetted width can be generated from high-resolution topography and hydraulic models. Note that neither objective involves a direct or indirect test of whether GCSs in fact explain past morphodynamic change that formed the current pattern or predict future changes driven by the current GCS. Before a study like that is attempted for a natural alluvial river, it is first necessary to evaluate if such a river even has coherent, self-organized GCSs. Thus, this study investigates the spatial structure of topographic variance in a river from base flow through large flood flows in its own right as the sensible first step.

176 The study site was a 6.4-km section of the lower Yuba River (LYR), an incising
177 and partially confined self-formed gravel-cobble bedded river (Figure 1; described in
178 Section 3). Several statistical tests were used on the serial correlation of minimum bed
179 elevation, Z, channel top width, W^j,and their geomorphic covariance structure,
180 $C(Z, W^j)$, where j indexes the flow discharge. The novelty of this study is that it provides
181 the first assessment of $C(Z, W^j)$ in a partially confined, self-maintained alluvial river
182 across a wide array of flows. The broader impact is that it provides a framework for
183 analyzing the flow dependent topographic variability of river corridors, without
184 differentiating between discrete landforms such as riffles and pools. Further, an
185 understanding of the flow dependent spatial structure of bed and width GCS would be
186 useful in assessing their utility in applied river corridor analysis and synthesis for river
187 engineering, management and restoration.
188
189 **2. Experimental Design**
190 This study aimed to deconstruct and reveal the coherent topographic structure of
191 a heterogeneous river valley as it existed at the moment of its mapping. This
192 understanding ought to inform both how the river arrived at this condition as well as how
193 it might change into the future, but this study does not involve analysis of
194 morphodynamic change to directly seek such linkages. To evaluate co-varying bed and
195 width undulations, the concepts and methods of geomorphic covariance structures
196 (GCSs) were used (Brown, 2014; Brown and Pasternack, 2014). Calculation of a GCS
197 from paired spatial series is straightforward by the cross product $x_{std,i} * y_{std,i,}$ where the
198 subscript std refers to standardized and possibly detrended values of two variables

199 x and y at location i along the centerline, creating the serial data set $C(X,Y)$. Since this
200 study is concerned with bed and flow dependent top width undulations, the GCS at each
201 flow j is denoted as $C(Z,W^j)$. More information on GCS theory is provided in section
202 4.2 below. GCS series were generated for eight flows ranging from 8.50 to 3,126 m^3/s,
203 spanning a broad range of flow frequency (Table 1). The range of selected flows spans
204 a low flow condition up to the flow of the last large flood in the river.-These flows were
205 selected to provide enough resolution to glean flow-dependent effects, while not
206 producing redundant results.
207 The first question this study sought to answer was if there was a tendency for
208 covarying $Z$and $W^j$and thus positive $C(Z,W^j)$, and how it changed with discharge. To
209 analyze this a histogram was generated for each flow dependent series of $C(Z,W^j)$ to
210 see if there was a tendency for positive $C(Z,W^j)$, and how that changed with flow The
211 second question was whether $C(Z,W^j)$ was random, constant, periodic or quasi-
212 periodic. Quasi-periodicity in this setting is defined as a series with periodic and
213 random components, as opposed to purely random or purely periodic (Richards,
214 1976a). Quasi-periodicity differs from periodic series in that the there are elements of
215 randomness blended in (Newland, 1993). To answer this question autocorrelation
216 function (ACF) and power spectral density (PSD) analyses of each $C(Z,W^j)$ series were
217 used to determine if there were quasi-periodic length scales at which $C(Z,W^j)$ covary
218 and how that changes with discharge.
219 Based on the studies listed above (Section 1.1), we hypothesize that gravel-cobble
220 bedded rivers capable of rejuvenating their riffle-pool relief should exhibit a topography
221 (at any instant in time) with a tendency for positive $C(Z,W^j)$ GCS. The basis for quasi-

222 periodic and positive $C(Z,W^j)$ is founded on the idea that, on average, channel
223 geometry is maintained during bankfull (e.g. geometric bankfull) discharge and that
224 locally channels are shaped by riffle-pool maintenance mechanisms (Wilkinson et al.
225 2004; MacWilliams et al., 2006; Caamano et al., 2009; Thompson, 2010). Based on the
226 literature reviewed in Section 1.1 we hypothesize that the $C(Z,W^j)$ GCS will, on
227 average, become more positive with increasing flow until approximately the bankfull
228 discharge, where the channel overtops its banks and non-alluvial floodplain features
229 exert control on cross-sectional mean hydraulics. At that point there may not be a
230 tendency for positive or negative residuals, if the topographic controls at that flood stage
231 are not important enough to control channel morphology. For example, smaller events
232 might occur frequently enough to erase the in-channel effects of the large infrequent
233 events, especially in a temperate climate (Wolman and Gerson, 1978). On the other
234 hand, if a system is dominated by the legacy of a massive historical flood and lacks the
235 capability to recover under more frequent floods, then the $C(Z,W^j)$ GCS will continue to
236 increase until the discharge that carved out the existent covarying bed and width
237 oscillations for the current topography is revealed. Note that we do not expect a clear
238 threshold where organization in the $C(Z,W^j)$ GCS is a maximum, but rather a range of
239 flows near the bankfull discharge. Given that the effect of a particular flow on a channel
240 is dependent not just on that flow, but the history of flow conditions that led to the
241 channel's condition (Yu and Wolman, 1987). Therefore, it should not be expected that
242 the observed patterns will be associated with a singular flow value. Also, this study
243 looked at a river in a Mediterranean climate, and thus it may be more prone to exhibiting
244 a wider range of positive $C(Z,W^j)$ GCS than a temperate or tropical river, as the

number and frequency of recovery processes is reduced (Wolman and Gerson, 1978). With this logic, it's hypothesized that the $C(Z, W^j)$ GCS will be quasi-periodic for flows near the bankfull discharge, due to the presence of bar and pool topography, and that the ACF and PSD will yield length scales commensurate with the average spacing of these topographic features. For flows above the bankfull discharge, a river corridor has many local alluvial landforms, bedrock outcrops and artificial structures on its floodplain and terraces. These features influence bed adjustment during floods that engage them, and hence impact the GCS. It is unknown how GCS length scales will change in response to the topographic steering these features induce causing changes to bed elevation, but investigating that is a novel and important aspect of this study. In addition to performing these tests we also present two ~ 1.4-km sections of the $C(Z, W^j)$ GCS, Z, W and the detrended topography for three representative flows to discuss specific examples of how these patterns change with landforms in the river corridor across a wide array of discharges.

Limitations to this study (but not the GCS approach) for worldwide generalization include not considering other variables relevant to how alluvial rivers adjust their shape, such as grain size, channel curvature and vegetation, to name a few. Some of these limitations were not study oversights, but reflected the reality that the study reach used had relatively homogenous sediments (Jackson et al., 2013), low sinuosity, and limited vegetation (Abu-Aly et al., 2014). This yielded an ideal setting to determine how much order was present for just bed elevation and channel width, but does not disregard the importance of these other controls, which can be addressed in future studies at suitable sites. Also, this study is not a direct test of the response to or drivers of morphodynamic

change. The extent to which GCS can be used as an indicator of change to greatly simply geomorphic analysis instead of doing morphodynamic modeling remains unknown, but finding metrics that link landforms, the agent that shape them, and the responses they induce has always been the goal of geomorphology (Davis, 1909).

3. Study Area

3.1 River context

The study area was the 6.4-km Timbuctoo Bend Reach of the lower Yuba River (LYR) in northeastern California, USA. The reach begins at the outlet of a bedrock canyon that is dammed ~ 3-km upstream, and the watershed above the dam drains 3480 km^2 of dry summer subtropical mountains. Little is known about the pre-European Yuba River, but the alluvial river in this reach is confined by valley hillsides and bedrock outcrops, and these are evident in some photos from early European settlers panning the river for gold in the late 1840s. During the mid to late 19^{th} century there was a period of extensive hydraulic gold mining of hillside alluvial deposits in the upper Yuba watershed that delivered an overwhelming load of heterogeneous sediment to the lowland river valley (James et al., 2009). Geomorphologist G. K. Gilbert photo documented the LYR around the time of its worst condition in the early 20^{th} century and provided foundational thinking related to how the river would evolve in time (Gilbert, 1917). In 1941 Englebright Dam was built to hold back further sediment export from the mountains, and that allowed the river valley to begin a process of natural recovery, which was reviewed by Adler (1980) and more recently by Ghoshal et al. (2010). However, this process was interfered with by widespread dredger mining in the early to

291 mid 20th century. In two locations of the study reach there are wide relict dredger tailings
292 piles on the inside of the two uppermost meander bends that the river has been
293 gradually eroding.
294 The hydrology of the regulated LYR is complex and quite different from the usual
295 story of significantly curtailed flows below a large dam. Englebright Dam primarily
296 serves as a sediment barrier and it is kept nearly full. As a result, it is operated to
297 overtop when outflow is > 127.4 m^3/s long enough to fill its small remaining capacity, so
298 flood hydrology is still seasonal and driven by rainfall and snowmelt in the watershed.
299 Two of three sub catchments do not have large dams, so winter floods and spring
300 snowmelt commonly cause spill over Englebright sufficient to exceed the bankfull
301 channel in Timbuctoo Bend. The one regulated sub catchment does have a large dam,
302 New Bullards Bar (closed in 1970), and this reduces the frequency and duration of
303 floodplain inundation compared to the pre-dam record (Escobar-Arias and Pasternack,
304 2011; Cienciala and Pasternack, in press), but not like other rivers where the entire
305 upstream watershed is regulated. Sawyer et al. (2010) reported the 1.5 year recurrence
306 interval for the post Englebright, pre New Bullards Bar period as 328.5 m^3/s and then for
307 post New Bullards Bar as 159.2 m^3/s. California has long been known to exhibit a
308 roughly decadal return period for societally important major floods that change river
309 courses (Guinn, 1890), though the magnitude of those floods is not necessarily a 10-
310 year recurrence interval scientifically. Since major flow regulation in 1970, the three
311 largest peak annual daily floods came roughly 10 years apart, in the 1986, 1997, and
312 2006 water years. The flood of 1997 was the largest of the post-dam record. The 2006
313 peak flood event had a recorded peak 15-minute discharge of 3126.2 m^3/s entering the

314 study reach.

315 Wyrick and Pasternack (2012) analyzed LYR inundation patterns in a high-
316 resolution DEM of the river produced after the 2006 wet season, and they considered
317 how channel and floodplain shapes change dramatically through the study reach. Their
318 findings apply to the Timbuctoo Bend Reach. Different locations exhibited spillage out of
319 the channel into low-lying peripheral swales and onto lateral and point bars at flows
320 from ~ 84.95-141.6 m^3/s. When the water stage rises to 141.6 m^3/s, relatively flat active
321 bar tops become inundated and the wetted extents line up with the base of willows
322 along steeper banks flanking the channel. These and other field indicators led to the
323 consideration of 141.6 m^3/s as representative of the bankfull discharge adjusted to the
324 modern regulated flow regime since 1970. By a flow of 198.2 m^3/s, banks are all
325 submerged and water is spilling out to various degrees onto the floodplain. The
326 floodplain is considered fully inundated when the discharge reaches 597.5 m^3/s. Above
327 that flow stage exist some terraces, bedrock outcrops, and soil-mantled hillsides that
328 become inundated. For the two relict dredger tailings piles mentioned earlier, they
329 interact with the flows ranging from 597.5-1,195 m^3/s. Apart from these piles, the flow
330 width interacts predominately with the valley walls for discharges at 1,195 m^3/s and
331 above. Given the estimate of bankfull discharge for the LYR, the instantaneous peak
332 flow during the 2006 flood was ~ 23 times that, so quite substantial compared to those
333 commonly investigated in modern geomorphic studies.

334

335 *3.2 Timbuctoo Bend details*

336 A lot is known about the geomorphology of Timbuctoo Bend, and this information

337 helps inform this study to substantiate the possibility that the river's topography is
338 organized in response to differential topographic steering as a function of flow stage.
339 According to Wyrick and Pasternack (2012), the reach has a mean bed slope of 0.2%, a
340 thalweg length of 6337 m, a mean bankfull width of 84 m, a mean floodway width of 134
341 m, an entrenchment ratio of 2.1 (defined per Rosgen, 1996), and a weighted mean
342 substrate size of 164 mm. Using the system of Rosgen (1996), it classifies as a B3c
343 stream, indicating moderate entrenchment and bed slope with cobble channel material.
344 A study of morphological units revealed that its base flow channel area consists of 20%
345 pool, 18% riffle, and then a mix of six other landform types. More than half of the area of
346 the riverbank ecotone inundated between base flow and bankfull flow is composed of
347 lateral bars, with the remaining area containing roughly similar areas of point bars,
348 medial bars, and swales (Wyrick and Pasternack, 2012). A study of bankfull channel
349 substrates found that they are differentiated by morphological unit type, but the median
350 size of all units is in the cobble range (Jackson et al., 2013)– even depositional bars,
351 which are often thought of as relatively fine in other contexts. Vegetated cover of the
352 river corridor ranged from 0.8 to 8.1% of the total wetted area at each flow, with more
353 inundated vegetation at higher flows.

354 White et al. (2010) used a sequence of historical aerial photos, wetted channel
355 polygons, repeat long profiles from 1999 and 2006, and a valley width series to
356 conclude that even though Timbuctoo Bend has incised significantly since 1942 in
357 response to many floods, there are several riffles and pools that persist in the same
358 wide valley locations, suggesting that valley width oscillations maintain those positions
359 and drive morphodynamic response. This suggests that it wouldn't matter exactly which

360 instant's topography one might analyze to look at the effect of topographic variability in
361 controlling or responding to large flood processes, as they all should reflect the same
362 topographic steering regime induced by the valley walls.
363 Two studies have been done to look at the hydraulic processes associated with
364 different flood stages in Timbuctoo Bend. Sawyer et al. (2010) found that one of the
365 pool-riffle-run units in this reach experienced flow convergence routing between
366 baseflow, bankfull flow, and a flow of roughly eight times bankfull discharge that
367 maintained riffle relief. Strom et al. (2016) assessed the hydraulics of the whole reach
368 over the same range of flows in this study, and they reported that the reach exhibits a
369 diversity of stage-dependent shifts in the locations and sizes of patches of peak velocity.
370 The spatial persistence of such patches decreased with discharge until flows exceeded
371 ~ 1000 m^3/s, at which point valley walls sustained their location for flows up to the peak
372 of 3,126 m^3/s. Also, peak-velocity patches resided preferentially over chute and riffle
373 landforms at within-bank flows, several morphological unit types landforms for small
374 floods, and pools for floods > 1000 m^3/s. These studies corroborate the process
375 inferences made by White et al. (2010) in that hydraulics were found to be stage-
376 dependent in ways that were consistent with the mechanism of flow convergence
377 routing.
378 Finally, Carley et al. (2012), Wyrick and Pasternack (2015), and Pasternack and
379 Wyrick (in press) used DEM differencing, uncertainty analysis, scale-stratified sediment
380 budgeting, and topographic change classification to analyze how the LYR changed from
381 1999-2008, including Timbuctoo Bend. These studies took advantage of the repeated
382 mapping of the LYR in 1999 and 2006-2008, with Timbuctoo Bend mapped entirely in

2006. They found large amounts of erosion and deposition, strong differential rates of change among different landforms at three spatial scales, and topographic changes driven by 19 different geomorphic processes. For Timbuctoo Bend, the dominant topographic change processes found were in-channel downcutting (including knickpoint migration) and overbank (i.e., floodplain) scour, with noncohesive bank migration a distant third. Thus, the river appears to change through adjustments to its bed elevation far more than changes to its width in this reach. This finding will come into play in interpreting the results of this study later on.

In summary, even with modern technology it is impossible to monitor the hydrogeomorphic mechanics of fluvial change in a large river for flows up to 22 times bankfull discharge, so recent studies have tried to get at the mechanisms during such events with a range of strategies. Historical river analysis, hydrodynamic modeling, and topographic change detection and analysis have been used together to reveal a picture of a river that is changing in response to multiple scales of landform heterogeneity that drive topographic steering. Even though the river has changed through time, there has been a persistence of nested landforms, and thus it would be useful to understand how topographic features are organized purely through an analysis of the DEM per the methods developed in this study. This study exclusively uses the 2006 map made during the dry season that followed the dramatic 2006 wet season, which included the large flood, two other notable peaks, and a total of 18 days of floodplain filling flow Thus it addresses the topography as it existed after that river-altering wet season and how it will in turn influence the dynamics of the next one.

406 **4. Methods**

407 To test the study hypotheses regarding the potential existence of geomorphic
408 covariance structures, Z and W^j series were extracted from the meter-scale topographic
409 map of Timbuctoo Bend produced from echosounder and robotic total station ground
410 surveys (Carley et al., 2012; see Supplemental Materials). A meter-scale 2D
411 hydrodynamic model was used to generate data sets for wetted width for each
412 discharge. Details about the 2D model are documented in the Supplemental Materials
413 and previous publications (Abu-Aly et al., 2013; Wyrick and Pasternack, 2014;
414 Pasternack et al., 2014); it was thoroughly validated for velocity vector and water
415 surface elevation metrics, yielding outcomes on par or better than other publications
416 using 2D models.

417

418 *4.1 Data Extraction*

419 A first step was to extract minimum bed elevation and top width spatial series
420 from the digital elevation model and 2D model outputs. This required having a sample
421 pathway along which bed elevation could be extracted from the DEM and top width from
422 the wetted extents from the 2D model. Sampling river widths was done using cross
423 sections generated at even intervals perpendicular to the sample pathway and then
424 clipped to the 2D model derived wetted extent for each flow. Because of this, the
425 pathway selected can have a significant bearing on whether or not sample sections
426 represent downstream oriented flow or overlap where pathway curvature is high. There
427 are several options in developing an appropriate pathway for sampling the river corridor.
428 The thalweg is commonly used in flow-independent geomorphic studies, but the thalweg

429 is too tortuous within the channel to adhere to a reasonable definition of top width.
430 Further, as flow increases, central flow pathway deviates from the deepest part of the
431 channel due to higher flow momentum and topographic steering from submerged and
432 partially submerged topography (Abu-Aly et al., 2014). Therefore, in this study we
433 manually developed flow-dependent sample pathways using 2D model hydraulic
434 outputs of depth, velocity and wetted area. The effect of having different sample
435 pathways for each flow is that it accounts for flow steering by topographic features in the
436 river corridor.

437 For each flow a grid of flow momentum ($d_i * {v_i}^2$) was generated in ARCGIS®,
438 where $d_i$is the depth and v_i is the velocity at node i in the 2D model hydraulics rasters.
439 Then a sample pathway was manually digitized using the momentum grid, following the
440 path of greatest momentum. For flow splits around islands, if the magnitude of
441 momentum in one channel was more than twice as great as the other it was chosen as
442 the main pathway. If they were approximately equal then the pathway was centered
443 between the split. Once a sample pathway was developed it was then smoothed using
444 a Bezier curve approach over a range of 100 m, or approximately a bankfull channel
445 width to help further minimize section overlaps. For each sample pathway cross
446 sections were generated at 5 m intervals and clipped to the wetted extent of each flow,
447 with any partially disconnected backwater or non downstream oriented areas manually
448 removed.

449 Despite smoothing there were areas of the river where the river has relatively
450 high curvature in the sample pathway causing sample section overlaps to occur. These
451 were manually edited by visually comparing the sample sections with the momentum

grid and removing overlapped sections that did not follow the downstream flow of water. This was more prevalent at the lower discharges than the higher ones due to the effects topographic steering creating more variable sample pathways.

To provide a constant frame of spatial reference for comparison of results between flows, while preserving flow-dependent widths, sections were mapped to the lowest flow's sample pathway using the spatial join function in ARCGIS®. The lowest flow was used, because that had the longest path. This insures no multiple-to-one averaging of data would happen, as that would otherwise occur if data were mapped from longer paths to shorter ones. To create evenly spaced spatial series the data was linearly interpolated to match the original sampling frequency of 5 m. For bed elevation, Z, the minimum value along each section was sampled from the DEM using the same sections for measuring width for the lowest flow sample pathway..

4.2 Developing geomorphic covariance structures

To generate GCS series for bed and flow-dependent width undulations the two variables, Z and W^j were first detrended and standardized. Detrending is not always needed for width in GCS analysis, but some analyses in this study did require it. Minimum bed elevation data, Z, were detrended using a linear model (Table 2) as is common in many studies that analyze reach scale bed variations (Melton, 1962, Richards, 1976a; McKean et al., 2008). Similarly, each flow dependent width series was linearly detrended, but the trends were extremely small, with a consistent slope of just 0.002 (Table 2). Finally, each series was standardized by the mean and variance of the entire detrended series (Salas et al., 1980) to achieve second order stationarity,

which is a prerequisite for spectral analysis. Second order stationarity of a series means that the mean and variance across the domain of analysis are constant (Newland, 1983). Removal of the lowest frequency of a signal, which can often be visually assessed, has little impact upon subsequent spectral analyses (Richards,1979). A linear trend was used over other options such as a polynomial, because a linear trend preserves the most amount of information in the bed series, while a polynomial can filter out potential oscillations. After detrended and standardized series of Z and W^jwere generated, then the GCS between them was computed by taking the product of the two at each centerline station, yielding a spatially explicit measure of how the two covary (Figure 2). The GCS is the whole series of $C(Z,W^j)$ values and not a single metric such as the traditional statistical definition of covariance. Interpretation of a GCS is based on the sign, which in turn is driven by the signs of contributing terms. For $C(Z,W^j)$, if both Z and W^j are positive or negative then $C(Z,W^j)>0$, but if only one is negative then $C(Z,W^j)<0$. For $C(Z,W^j)$ these considerations yield four sub-reach scale landform end members that deviate from normative conditions (Figure 3). Normal conditions in this context refer to areas where both variables are close to the mean and thus $C(Z,W^j)\sim 0$. These landforms are not the same as classic zero-crossing riffles and pools (e.g. Carling and Orr, 2000), because they explicitly account for bed and width variation. Neither are they the same as laterally explicit morphological units (Wyrick and Pasternack, 2014), because they average across the full channel width. Also, both of those types of landforms are flow independent, whereas the landforms identified herein are expressly flow-dependent, reflecting the entire cross sectional topography at a given flow. Note that the signs of Z and $W^j$are not only important, but the magnitude is, too.

Since $C(Z, W^j)$ is generated by multiplication, if either Z or W^j is within the range of -1 to 1, then it serves to discount the other. If Z or W^j is > 1 or < -1 it amplifies $C(Z, W^j)$. We did not assess the statistical significance of coherent landform patterns, but one could do so following Brown and Pasternack (2014).

4.3 Data Analysis

Before any statistical tests were performed we first visually assessed the data in two approximately 1.4-km long sections to illustrate how $C(Z, W^j)$ is affected by flow responses to landforms. For these two examples only three discharges were selected to illustrate flow dependent changes in Z, W^j, and $C(Z, W^j)$ with fluvial landforms. The lowest and highest flows, e.g. 8.50 and 3,126 m^3/s, were selected to bracket the range of flows investigated. The intermediate flow selected was 283.2 m^3/s based on the shifts in $C(Z, W^j)$ observed in the histogram, ACF and PSD tests as shown below in the results. For these examples the exact magnitudes of $C(Z, W^j)$ are not as important as the patterns and how they relate to visually discernible landforms.

A Mann-Whitney U-test was performed between each $C(Z, W^j)$ dataset to determine if they were statistically different at the 95% level. Histograms were then computed for each $C(Z, W^j)$ dataset to evaluate whether there was a tendency for the data to be positively covarying and how that changes with discharge. Two histograms were developed, one based on the quadrant classification of $C(Z, W^j)$ for each flow and another showing the $C(Z, W^j)$ magnitude. This was done so that the distribution of both the type of $C(Z, W^j)$ and magnitudes could be assessed. Additionally, the bivariate Pearson's correlation coefficients (r) were computed between Z and W^j to assess their

potential interdependence. Bivariate Pearson's correlation coefficients were also computed each series of W^j. Statistical significance was assessed for (r) using a white noise null hypothesis at the 95% level.

Next, ACF and PSD analyses were used to determine if $C(Z, W^j)$ was quasi-periodic or random, as it was visually evident that it was not constant or strictly periodic. If a series is quasi-periodic this will be reflected in statistically significant periodicity in the ACF (Newland, 1993; Carling and Orr, 2000). Because the PSD is derived from the ACF the two tests show the same information, but in different domains, with the ACF in the space domain and the PSD in the frequency domain. So while the ACF analysis reveals periodicity in the signal (if present), the PSD analysis presents the associated frequencies. Both are shown to visually reinforce the results of the PSD analysis. This is helpful because spectral analysis can be very sensitive to the algorithm used and associated parameters such as window type and size. Showing the ACF allows a visual check of dominant length scales that may have quasi-periodicity. The ACF analysis was performed for each flow dependent series of $C(Z, W^j)$ and then these were compared among flows to characterize stage dependent variability and to analyze how spatial structure changed with discharge. This test essentially determines the distances over which $C(Z, W^j)$ are similar. An unbiased estimate of autocorrelation for lags was used:

$$R_k = \frac{\frac{1}{\mathrm{n-k}}\sum_{\mathrm{i=1}}^{\mathrm{n-k}}(x_i-\bar{x})(x_{i+k}-\bar{x})}{\frac{1}{\mathrm{n}}\sum_{\mathrm{i=1}}^{\mathrm{n-k}}(x_i-\bar{x})^2} \quad (1)$$

where x_i is a value of a GCS series at location i, $\bar{x}$ is the mean value of the GCS (zero due to standardization process) and the terms $\frac{1}{\mathrm{n-k}}$ and $\frac{1}{\mathrm{n}}$ account for sample bias (Cox, 1983; Shumway and Stoffer, 2006). Each R_k versus lag series was plotted against

543 discharge for a maximum of 640 lags (3.2 km, or approximately half the study length),
544 creating a surface that shows how ACF evolves with flow. Lag intervals are equal to
545 sample interval for the datasets (e.g. 5 m). Statistical significance was assessed relative
546 to both white and red noise autocorrelations. White noise is associated with random
547 processes that are uncorrelated in space, while red noise is associated with data that
548 has properties of 1st order autocorrelation (Newland, 1993). The benefit of this approach
549 is that (i) many fluvial geomorphic spatial series display autoregressive properties
550 (Melton, 1962; Rendell and Alexander, 1979; Knighton, 1983; Madej, 2001) and (ii) it
551 provides further context for interpreting results beyond assuming white noise properties.
552 The 95% confidence limits for white noise are given by $-\frac{1}{n}+/-\frac{2}{\sqrt{n}}$ (Salas et al., 1980).
553 For red noise, a first order autoregressive (AR1) model was fit to the standardized
554 residuals for each spatial series of bed elevation and channel width. For comparison,
555 first order autoregressive (AR1) models were produced for 100 random spatial series
556 (each with the same number of points as the flow width spatial series) and averaged.
557 Each averaged AR1 flow width series was then multiplied against the AR1 bed elevation
558 series to create an AR1 model for each $C(Z,W^j)$. The red noise estimate was then
559 taken as the average of all AR1 models of $C(Z,W^j)$. The ACF plots were made so that
560 values not exceeding the white noise significance are not shown, along with a reference
561 contour for the AR1 estimate. Frequencies can be gleaned from the ACF analysis by
562 taking the inverse of the lag distance associated repeating peaks following Carling and
563 Orr (2002).
564 Power spectral density was estimated for each $C(Z,W^j)$ series using a modified
565 periodogram method as an additional test for periodicity (Carter et al., 1973). The

566 periodogram is the Fourier transform of the biased estimate of the autocorrelation
567 sequence. The periodogram is defined as:

568 $$P(f) = \frac{\Delta x}{N}\left|\sum_{n=0}^{N-1} h_n x_n e^{-i2\pi f n}\right|^2 \quad (2)$$

569 where $P(f)$ is the power spectral density of x, h_n is the window, Δx is the sample rate,
570 and N is the number of data data points (Trauth et al., 2006). While the raw
571 periodogram can exhibit spectral leakage, a window can reduce this effect. A hamming
572 window was used with a length equal to each data set. Since samples were taken every
573 5 m, this resulted in a sampling frequency of 0.2 cycles/m, and a Nyquist frequency, or
574 cutoff of 0.1 cycles/m. The number of data points used for the analysis was roughly half
575 the largest data set, resulting in a bandwidth of 0.00016 cycles/m. For PSD estimates a
576 modified Lomb-Scargle confidence limit for white noise at the 95% level was used as
577 recommended by Hernandez (1996). Since this study was concerned with changes in
578 PSD with flow, estimates were plotted relative to the standard deviation of all PSD
579 results for all series. This was done instead of using the standard deviation of each
580 series, because that erroneously inflates power within a series without context for the
581 variance of adjacent flows.
582

583 **5. Results**

584 *5.1 Relating $C(Z, W^j)$ patterns to landforms*

585 The first example is located at the lower end of the study area and transitions from a
586 valley meander to a straighter valley section with several valley corridor oscillations
587 (Figure 4). Starting upstream there is a large point bar on river left with a pool (i.e., $-Z$)
588 that transitions to a broad riffle with a 200 m long zone with Z > 1. Downstream the river

589 channel impinges on the valley walls creating two forced pools with localized negative
590 spikes in Z (Figure 4A,B). Downstream of this the low flow channel is steered to the left
591 of the valley, being bounded by two bars. Relative bed elevations in this zone have
592 positive Z values near 1. Past this there is an inset anabranch that transitions to a
593 constricted pool with a broad terrace on river left. Relative bed elevations in this lower
594 zone fluctuate between 0 and -1.

595 Given that bed elevation is held fixed for this type of analysis, changes in relative
596 flow width with discharge act to modulate the sign and magnitude of the $C(Z, W^j)$ GCS
597 with increasing flow. In particular, when Z is near a value of 1, the relative flow W
598 modulates the GCS signal, with several possible changes including persistence,
599 shifting, reversal, and emergence. For example, a persistent positive W oscillation
600 occurs above the broad riffle near station 1300, where this zone is always relatively
601 wide regardless of flow. The anabranch zone however, shows the positive peak in W
602 shift downstream from station 900 to 600 from 8.5 to 283.2 m^3/s. Two reversals in
603 relative flow width occur from low to high flow near stations 350 and 1100, which also
604 create reversals in the GCS, but with different signs. Near station 350 Z and W are
605 negative at 8.5 and 283.2 m^3/s creating a positive GCS. However, W increases with
606 flow discharge with an emergent positive peak in W at 3,126 m^3/s, creating a negative
607 GCS.

608 At 8.5 m^3/s zones of high relative flow width are located above zones of positive Z,
609 such as near stations 800 and 1300. As flow increases to 283.2 m^3/s these areas
610 continue to amplify in magnitude becoming relatively wider, however the patterns are
611 slightly different. Relative flow widths at the broad riffle near station 1300 increase

612 upstream of the zone of positive Z, whereas for the anabranch near station 800 the
613 peak in relative width shifts downstream ~200 m. At 3126 m^3/s the valley walls are fully
614 engaged in this location and there are three oscillations in W with positive peaks
615 centered near 300, 1100 and 1500 (Figure 4D).
616 The other example area occurs at a transition from a valley bend to a straighter
617 section where the river transitions from a broad point bar on river left and eventually
618 crosses over between two smaller inset point bars (Figure5A,B). Starting at the
619 upstream extent a large point bar is located on river left with two forced pools in the
620 channel at approximately 3500 and 3600 with the strongest negative spikes in Z (Figure
621 5C,D). Downstream where the point bar ends the bed profile increases with a high
622 magnitude peak (e.g. Z >1) over a broad riffle located above 3000. As mentioned
623 above in Section 3, this pool-riffle-run sequence was studied in great detail by Sawyer
624 et al. (2010), who confirmed the occurrence of naturally rejuvenating riffle-pool
625 topography. Immediately below the broad riffle is a localized zone where $Z < 1$
626 adjacent to a small bedrock outcrop. Within the alternate bars the bed profile is
627 between 0 and 1 for ~ 300 m, followed by a localized negative peak in Z around station
628 2300.
629 For the first 200 m W is < 0 for all three flows, but gradually increases downstream
630 with increasing flow (Figure 5C). The two deep pools in this initial zone have $Z < 1$, so
631 the GCS is >1 for all flows but reaches a maximum magnitude of 6 at 283.2 m^3/s.
632 Beyond this area W increases for all flows, but the relative peak broadens and shifts
633 downstream with increasing discharge. At 8.5 m^3/s the peak is centered near station ~
634 3000 where it appears a backwater increases flow widths upstream of station 2900. For

283.2 m^3/s the peak shifts downstream ~ 150 m as the anabranch becomes activated and begins to spread water out. At 3126 m^3/s the peak is shifted another ~ 300 m downstream as the bounding point bars are inundated. These shifts in relative W act with the bed profile to create a sharper positive peak in $C(Z, W^j)$ near the riffle at low flows, but then this peak dampens and shifts downstream with increasing flow. Given that the lower ~ 500 m of this example area have Z ~ 0 the $C(Z, W^j)$, GCS is also ~ 0.

Overall both examples show that zones where Z was either > 1 or < -1 were associated with large pools and riffles in the study area, and were characterized by strong peaks (e.g. >1) in $C(Z, W^j)$. An interesting result is that most of the locations where Z <1 were short in length, whereas areas where $Z > 1$ tended to be broader in length.

5.2 Is there a tendency for positively covarying bed and width oscillations?

The histogram of $C(Z, W^j)$ showed that regardless of discharge, there was a tendency for positive values, and that this changed with stage (Figure 6A). At least 55% of the data always had $C(Z, W^j) > 0$, increasing to 68% at 283.2 m^3/s, and then slightly declining beyond this flow and stabilizing around 60% (Figure 6). There were at most 5% of values < -1, with an average and standard deviation of 3% and 2%, respectively. Contrasting this, values > 1 peaked at 35% at 141.6 m^3/s and declined with increasing discharge. So out of the two extremes, the data exhibited a tendency for positive values, with negative values < -1 being very rare.

The Mann Whitney U-test showed interesting flow dependent aspects of the $C(Z, W^j)$ data sets, where some ranges of flows were significantly different from each

658 other, and others being similar (Table 3). For example, the 8.50 m^3/s $C(Z, W^j)$ had p
659 values that were all significant at the 95% level for each other flow, indicating
660 differences in their distributions. For flows between 28.3-597.5 m^3/s, the p values
661 indicated that the series were statistically similar, but not for higher flows. The p values
662 for 1,195, 2,390, and 3,126 m^3/s were statistically similar at the 95% level, but not for
663 lower flows.

664 The quadrant-based histogram reveals further insight into the distribution of river
665 geometry with flow (Figure 6B). The average percentage of $C(Z, W^j)$ for each quadrant
666 across all flows was 30% $\{+W, +Z\}$, 14% $\{+W, -Z\}$, 25% $\{-W, +Z\}$, and 31%
667 $\{-W, -Z\}$, with standard deviations ranging from 2-3%. Percentages of positive
668 $C(Z, W^j)$ was relatively evenly distributed between $\{+W, +Z\}$ and $\{-W, -Z\}$, although
669 the latter was slightly more prevalent. The percent of the data in the $\{+W, +Z\}$ quadrant
670 increased from 26% at 8.50 m^3/s, peaked at 34% at 597.5 m^3/s, decreased to 30% at
671 1195 m^3/s and stabilized near this value for higher flows. Meanwhile, the percent of the
672 data in the $\{-W, -Z\}$ quadrant increased from 29% at 8.50 m^3/s and peaked at 35% at
673 141.6 - 283.2 m^3/s flow, and then decreased to 30% at 597.5 m^3/s. After that it
674 increased to 33% and stabilized at and beyond 1,195 m^3/s. Both the $\{+W, -Z\}$ and
675 $\{+W, -Z\}$ quadrants followed a similar but opposite trend, reaching a minimum at 283.2
676 m^3/s.

677 Further insights into the positive nature of $C(Z, W^j)$ can be inferred from bivariate
678 Pearsons correlation coefficients of Z and W^j(Figure 7). Similar to $C(Z, W^j)$ the flow
679 dependent response was that the correlation between Z and W^j increased with flow
680 until 283.2 to 597.5 m^3/s and then subsequently declined. To further reinforce these

results one can also inspect the plot of Z,W^j and $C(Z,W^j)$ for 283.2 m^3/s, visually showing the synchronous nature of Z and W^j (Figure 2) The correlations between combinations of W^j show that each series is significantly correlated to the next highest flow, but there is an interesting flow dependent pattern (Figure 8). Correlations between series decrease with increasing flow, reaching a minimum between 597.5 and 1195 m^3/s, and then increasing again.

5.3 Are bed and width oscillations quasi-periodic?

The ACF of $C(Z,W^j)$ also showed similar changes with discharge as the above analyses with increases in the presence and magnitude of autocorrelation from 8.50 to 597.5 m^3/s and then subsequent decline with increasing flow (Figure 9A). At the lowest discharge there are approximately two broad bands of positive autocorrelation that exceeded both the white noise and AR1 threshold at lag distances of 1400 and 2100 m. At 28.32 m^3/s these three peaks broaden and the highest correlation was found at lag distance 1400 m, which increased from ~0.38 to 0.65. At the bankfull discharge of 141.6 m^3/s the peak at 1400m diminishes, while the peak near 2100 m increased in strength (e.g. correlation magnitude). At 283.2 m^3/s there are still peaks near 1400 and 2100 mthat exceed both white noise and the AR1 threshold,but two other significant peaks emerge near 700 and 2800 m. Similar statistically significant correlations are found at 596.5 m^3/s, albeit narrower bands of correlation. The correlation distances at 283.2 and 596.5 m^3/s average ~700 m, and this would have a frequency of approximately 0.0014 cycles/m. Beyond 596.5 m^3/s the ACF diminishes rapidly with no peaks that are statistically significant compared to red noise. Overall, the ACF results show that

704 $C(Z, W^j)$ is quasi-periodic from 8.50 m^3/s to 141.6-597.5 m^3/s, but then the periodicity
705 decreases in strength as flow increased.
706 Similar to ACF analysis, PSD analysis showed quasi-periodic components of
707 $C(Z, W^j)$ exhibiting flow dependent behavior (Figure 9B). For 8.50-283.2 m^3/s there is a
708 high power band (e.g. PSD/σ ~12-16) centered on 0.0014 cycles/m, which is confirmed
709 from the ACF analysis above. For 8.50 -141.6 m^3/s there are also smaller magnitude
710 peaks ranging from 3-8, spread out over several frequencies. There's also a high
711 magnitide component at the lowest frequency band that emerges at 28.32 and declines
712 by 283.2 m^3/s. These low frequency components are commonly associated with first
713 order auto-regressive behavior in the data (Shumway and Stoffer, 2010). At 597.5 m^3/s
714 power is still associated on 0.0014 cycles/m, albeit with a ~50% reduction in magnitude.
715 Beyond this flow the frequency range and magnitude of statistically significant values
716 declines with discharge. Overall, both ACF and PSD results show that $C(Z, W^j)$ is
717 quasi-periodic from 8.50 m^3/s to 283.2 m^3/s but then decreased in strength as flow
718 increased. Further, the PSD results show that the $C(Z, W^j)$ GCS is flow dependent and
719 multiscalar, being characterized by a range of statistically significant frequencies.
720
721 **6. Discussion**
722 *6.1 Coherent undulations in cobble-gravel bed river topography*
723 The primary result of this study is that in an incising, partly confined, regulated
724 cobble-gravel river whose flow regime is dynamic enough to afford it the capability to
725 rejuvenate its landforms, there was a tendency for positive $C(Z, W^j)$ and thus covarying
726 Z and W amongst all flows analyzed. Based on the ACF and PSD analyses the

727 $C(Z, W^j)$ GCS undulations are quasi-periodic. The results of this study associated
728 channel organization across a range of recurrence intervals frequencies within the
729 range of commonly reported channel forming discharges for Western U.S. rivers (e.g.,
730 1.2-2.5 years) as well as substantially larger flows. These conclusions are obviously
731 limited to the study reach, but this should not prohibit discussing possible mechanisms
732 that could lead to these observed patterns, as well as the role of variable flows and
733 incision.

734 Most notably, the test river exhibited a dominance of positively covarying values
735 of $C(Z, W^j)$ across all flows, being characterized by an quasi-periodic pattern of wide
736 and shallow or narrow and deep cross sections. This supports the idea that alluvial river
737 reaches have a tendency for adapting wide and shallow and narrow and deep cross
738 sections to convey water flow (Huang et al., 2004). Rather than select a single type of
739 cross section to maximize energy dissipation to create a uniform cross section geometry
740 at a single channel maintaining flow, commonly referred to as bankfull, it appears that
741 alluvial rivers adjust their channel topography to have cross sections that roughly
742 alternate between those that are wide and shallow and narrow and deep (Figure 6B;
743 Huang et al., 2004), with some locations having a prismatic channel form indicative of
744 normative conditions, particularly in transition zones. Whether this is attributed to
745 minimizing the time rate of potential energy expenditure per unit mass within a reach
746 (Langbein and Leopold, 1962; Yang, 1971; Cherkauer, 1973; Wohl et al., 1999) or
747 channel unit scale mechanisms associated with riffle-pool maintenance (Wilkinson et al.
748 2004; MacWilliams et al., 2006; Caamano et al., 2009; Thompson, 2010;) remains to be
749 determined. Given that extremal hypotheses and riffle-pool maintenance act at different,

750 yet interdependent scales, it is likely that both play an intertwined and inseparable role
751 in channel form. That said, extremal theories are limited to predicting mean channel
752 conditions within a reach (Huang et al., 2014), with no models that can yet fully predict
753 sub-reach scale alluvial river topography, so we turn our attention to more tractable
754 hydrogeomorphic processes related to riffle and pool topography.
755 Presumably, the quasi-oscillatory $C(Z, W^j)$ GCS pattern is also linked to flow
756 dependent patterns of convective acceleration and deceleration zones (Marquis and
757 Roy, 2011; MacVicar and Rennie, 2012), as the length scales of the GCS were aligned
758 with the spacing of erosional and depositional landforms such as bars and pools. This
759 aspect is supported by ACF and PSD results as well as other two studies on the test
760 reach. First, it appears that the quasi-periodicity of the $C(Z, W^j)$ GCS is related to the
761 pool-riffle oscillation in the river corridor. The PSD analysis showed that the dominant
762 frequency of $C(Z, W^j)$ was ~ 0.0014 cycles/m, which equates to a length scale of ~ 700
763 m (Figure 9). Three of the morphologic units (MUs) studied by Wyrick and Pasternack
764 (2014) can be used for context including pools, riffles, and point bars. In their results for
765 the Timbuctoo Bend Reach, pools, riffles, and point bars had an average frequency of
766 0.0029, 0.0028, and 0.001 cycles/m. Considering that pools and riffles are defined as
767 two end-members of positive $C(Z, W^j)$, then the frequency of riffles and pools should be
768 twice that of the $C(Z, W^j)$ GCS as found herein. That is, a single oscillation of $C(Z, W^j)$
769 GCS would include both a narrow and deep (e.g. pool) and a wide and shallow (e.g.
770 riffle) geometries, although transitional forms are possible within a cycle, too (Figure 3).
771 Therefore, it appears that the quasi-periodicity of the $C(Z, W^j)$ GCS is related to the
772 pool-riffle oscillation in the river corridor. This is in agreement with studies based on field

773 investigations and numerical models that relate this observation to quasi-periodic bed
774 and width variations associated with bar-pool topography (Richards, 1976b; Repetto
775 and Tubino, 2001; Carling and Orr, 2002).
776 Second, Sawyer et al. (2010) showed that stage dependent flow convergence
777 maintained bed relief by topographically mediated changes in peak velocity and shear
778 stress at the central riffle in second example (Figure 5). Interestingly, the flow width
779 series phases relative to bed elevations in accordance with theory (Wilkinson et al.,
780 2004) and field and numerical studies (Brown and Pasternack, 2014). This supports an
781 already reported relationship between the $C(Z, W^j)$ GCS and the process of flow
782 convergence routing (Brown and Pasternack, 2014 Brown et al., 2016).
783 Lastly, Strom and Pasternack (2016) showed that peak zones of velocity undergo
784 variable changes in their location with discharge, with most velocity reversals occurring
785 after 597.5 m^3/s. In this case the zones of peak velocity patches underwent complex
786 changes from being associated with narrow topographic high points at base flows
787 $(-W^j, +Z)$ to topographic low points where flow width is constricted at high flows
788 $(-W^j, -Z)$. Overall, the presence of oscillating wide and shallow and narrow and deep
789 cross sections appears to be linked to hydrogeomorphic processes of riffle-pool
790 maintenance.
791
792 *6.2* Hierarchical nesting, variable flows and the role of incision
793 This study quantitatively supports the idea that river morphology in partially confined
794 valleys is hierarchically nested with broader exogenic constraints such as the bedrock
795 valley walls, as well as channel width scale alluvial controls such as point bars and

islands. Our study quantitatively characterized interesting shifts in the amount of correlation amongst flow width series and in the presence of quasi-periodic oscillations in $C(Z, W^j)$ with changes in flow. Each series of W^j were significantly correlated with the next highest flow, but this was lowest between 597.5 and 1195 m^3/s, where the valley walls begin to be engaged (Figure 7). Further, both the ACF and PSD show that quasi-periodicity in $C(Z, W^j)$ declines after 597.5 m^3/s (Figure 9). In addition, Strom and Pasternack (2016) showed that reversals in peak velocity occur when flows exceed 597.5 m^3/s. While results show that statistically significant correlations between Z and W^j occur for a range of flows, the greatest magnitude is not when the valley walls are inundated, but for the 283.2 m^3/s channel and incipient floodplain. Given that correlations were still significant for the flows that inundate the valley walls, this does not refute the role of valley width oscillations in potentially controlling riffle persistence (White et al., 2010), but rather adds new insight to the morphodynamics of rivers incising in partially confined valleys. This suggests that the incision process may be decoupling the organization of the riverbed away from being controlled by the valley walls and instead phased towards reshaping channel topography within the inset bars that are nested within the valley walls. As the riverbed incises further down through knickpoint migration (Carley et al., 2012) this may act to shift zones of high and low wetted width upstream unless lateral erosion can keep pace.

6.3 Broader Implications

This study quantified relationships between flow width and minimum bed elevation in a partly confined and incising gravel-cobble bedded river, as well as for the first time

819 how they change with stage. While study results are currently limited to rivers similar to
820 the study reach, there are several key results of this study that may have broader
821 relevance to river restoration and management.
822 First, a key result of this study was that channel geometry was organized into
823 positively covering bed and width undulations across all flows analyzed, alternating
824 between wide and shallow and narrow and deep cross sections. This is a very different
825 view from the classical definition of singular and modal bankfull channel geometry often
826 used to guide river and stream restoration (Shields et al., 2003). Instead, our study
827 found that channel geometry at all flows had a relatively even mixture of wide and
828 shallow and narrow and deep cross sections. Studies that deconstruct the complexity
829 of river channel geometry to modal ranges of channel width and depth have always
830 shown scatter, which has mostly been attributed to measurement uncertainty and/or
831 local conditions (Park, 1977; Philips and Harman, 1984; Harman et al., 2008; Surian et
832 al., 2009). Our study suggests that this variability is a fundamental component of
833 alluvial river geometry. While this concept was proposed by Hey and Thorne (1983)
834 over two decades ago, few studies have integrated these ideas into river engineering
835 and design (e.g. see Simon et al., 2007). Thus, this study further supports a needed
836 shift away from designing rivers with modal conditions to designing rivers with quasi-
837 oscillatory and structured variations in channel topography (Brown et al., 2016).
838 Second, this study has implications to restoration design and flow reregulation in that
839 a wide array of discharges beyond a single channel forming flow are presumably
840 needed for alluvial channel maintenance (Parker et al., 2003). Commonly singular
841 values of channel forming discharge, usually either bankfull or effective discharge, are

used in stream and river restoration designs (Shields et al., 2007; Doyle et al., 2007). This study refutes this concept for rivers such as studied herein, as supported by the results that show gradual changes in channel organization within a band of discharges with recurrence intervals ranging from 1.2-5 years, and four fold range in absolute discharges. Instead, stream and river restoration practitioners should analyze ranges of flow discharges and the potential topographic features (existing or designed) that could invoke stage-dependent hydrodynamic and geomorphic processes associated with complex, self maintaining natural rivers.

Third, while the length scales of covarying bed and width undulations are approximate to the spacing of bars and pools in the study area, they are quite complex and lack explicit cutoffs that illustrate power in a singular frequency band. Thus, river restoration efforts that specify modal values of bedforms may overly simplify the physical structure of rivers with unknown consequences to ecological communities and key functions that are the focus of such efforts. River restoration designs need to mimic the multiscalar nature of self-formed topography by incorporating GCS into river engineering (Brown et al., 2014) or somehow insure that simpler uniscalar designs will actually evolve into multiscaler ones given available flows and anthropogenic boundary constraints.

Fourth, this study has potential implications for analyzing the effect of flow dependent responses to topography and physical habitat in river corridors. Valley and channel widths have shown to be very predictive in predicting the intrinsic potential of salmon habitat (Burnett et al., 2007). Further, the role of covarying bed and width undulations in modulating velocity signals and topographic change has implications to the

maintenance of geomorphic domains used by aquatic organisms. As one example, consider that adult salmonids use positively covarying zones such as riffles (e.g. $+W^j, +Z$) for spawning and pools (e.g. -$W^j, -Z$) for holding (Bjorn and Reiser, 1991). In the study reach Pasternack et al. (2014) showed that 77% of spawning occurred in riffles and chute morphologic units, which are at or adjacent to areas where $C(Z, W^j)$>1 (Figure 4, Figure 5), supporting this idea. The presence and structure of covarying bed and width undulations is also thought to be important indirectly for juvenile salmonids that require shallow and low velocity zones for refugia during large floods. For example, the expansions that occur at the head of riffles would presumably provide lateral zones of shallow depths and moderate velocities needed for flood refugia. In the absence of positive bed relief, and zones of $+W, +Z$, flow refugia zones would be hydrologically disconnected from overbank areas, impacting the ability of juvenile salmon to utilize these areas as refugia during floods and potentially leading to population level declines (Nickelson et al., 1992). Future work should better constrain the utility of GCS concepts in assessing aquatic habitat.

Lastly, it is possible that the $C(Z, W^j)$ GCS could be used as a comparative proxy in remote sensing applications to determine how the topographic structure of rivers change with flow, and how that may also change though time. The zoomed examples of $C(Z, W^j)$ and the detrended river topography highlight how this type of GCS can be used to characterize the topographic influence on wetted width and bed elevation variability in river corridors. The $C(Z, W^j)$ GCS may be used diagnostically to assess riverine structure and hydraulic function in a continuous manner within a river across an array of flows. While not studied herein, prior work (Brown and Pasternack, 2014)

888 showed that the magnitude of $C(Z, W^j)$ can also be related to flow velocity, though
889 lagged effects do occur. Since the magnitudes can be linked to both unique landforms
890 and flow velocity they may have utility in assessing topographic and hydraulic controls
891 in river corridors.

892 LiDAR and analytical methods for developing bed topography in rivers has improved
893 considerably (McKean et al, 2009). For example, Gessese et al. (2011) derived an
894 analytical expression for determining bed topography from water surface elevations,
895 which can be obtained from LiDAR (Magirl et al, 2005). Assuming one has an adequate
896 topographic data set, whether numerical flow modeling is needed to generate wetted
897 width data sets places a considerable constraint on performing this type of analysis.
898 This could potentially be relaxed, especially at flows above bankfull, using a constant
899 water slope approximation for various flow stages. At smaller discharges in rivers there
900 are typically defects in the water surface elevation, where the bed topography exerts a
901 strong control on bed elevations (e.g. Brown and Pasternack, 2008). However, many
902 studies suggest that on large alluvial rivers bankfull and flood profiles show that they
903 generally flatten and smoothen once bed forms and large roughness elements such as
904 gravel bars are effectively submerged. In this case, one can then detrend the river
905 corridor and take serial width measurements associated at various heights above the
906 riverbed (Gangodagamage et al., 2007). The height above the river then can then be
907 related to estimates of flow discharge and frequency, so that the change GCS structure
908 can be related to watershed hydrology (Jones, 2006). There's also the obvious option of
909 using paired aerial photography with known river flows by correlating discharge with
910 imagery dates and widths. Future work should constrain whether similar conclusions

911 can be reached using field and model derived estimates of wetted width as opposed to
912 modeled solutions.
913
914 **7. Conclusions**
915 A key conclusion is that the test river exhibited positively covaring oscillations of bed
916 elevation and channel width across all flows analyzed. These covarying oscillations
917 were found to be quasi-periodic at channel forming flows, scaling with the length scales
918 of pools and riffles. Thus it appears that alluvial rivers organize their topography to
919 have oscillating shallow and wide and narrow and deep cross section geometry, even
920 despite ongoing incision. Presumably these covarying oscillations are linked to
921 hydrogeomorphic mechanisms associated with alluvial river channel maintenance. As
922 an analytical tool, the GCS concepts in here treat the topography of river corridors as
923 system, which is thought of as an essential view in linking physical and ecological
924 processes in river corridors at multiple scales (Fausch et al., 2002; Carbonneau et al.,
925 2012). While much research is needed to validate the utility of these ideas to these
926 broader concepts and applications in ecology and geomorphology, the idea of GCS's,
927 especially for width and bed elevation, holds promise.
928
929 **8. Data Availability**
930 Each $C(Z, W^j)$ dataset is available from either author by request.
931
932 **9. Acknowledgements**
933 Although not directly funded by any source, this study used data and models

from studies previously sponsored by Pacific Gas & Electric Company, the U.S. Fish and Wildlife Service Anadromous Fish Restoration Program, Yuba County Water Agency, and the Yuba Accord River Management Team. Co-author G.B. Pasternack received support from the USDA National Institute of Food and Agriculture, Hatch project number #CA-D-LAW-7034-H.

10. References

Abu-Aly TR, Pasternack GB, Wyrick JR, Barker R, Massa D, Johnson T. 2014. Effects of LiDAR-derived, spatially distributed vegetation roughness on two-dimensional hydraulics in a gravel-cobble river at flows of 0.2 to 20 times bankfull. Geomorphology 206: 468-482. DOI: 10.1016/j.geomorph.2013.10.017

Adler, LL. 1980. Adjustment of Yuba River, California, to the influx of hydraulic mining debris, 1849–1979. M.A. thesis, Geography Department, University of California, Los Angeles.

Andrews ED. 1980. Effective and bankfull discharges of streams in the Yampa River basin, Colorado and Wyoming. Journal of Hydrology 46: 311-330.

Bjorn TC, Reiser DW. 1991 Habitat Requirements of Salmonids in Streams. In: Influences of Forest and Rangeland Management on Salmonid Fishes and Their Habitats. Edited by W.R. Meehan. Special Publication 19. American Fisheries Society. Bethesda, MD. pp. 83-138.

Brown RA. 2014. The Analysis and Synthesis of River Topography (Doctoral Dissertation) University Of California, Davis. 187 pages.

Brown RA, Pasternack, GB. 2008. Engineered channel controls limiting spawning habitat rehabilitation success on regulated gravel-bed rivers. Geomorphology 97: 631–654.

Brown RA, Pasternack GB. 2014. Hydrologic and Topographic Variability Modulate Channel Change in Mountain Rivers. Journal of Hydrology 510: 551–564.DOI: 10.1016/j.jhydrol.2013.12.048

Brown, R.A., Pasternack, G.B., Wallender, W.W., 2014. Synthetic River Valleys: Creating Prescribed Topography for Form-Process Inquiry and River Rehabilitation Design. Geomorphology 214.

965 Brown, R.A., Pasternack, G.B., Lin, T., 2016. The topographic design of river channels
966 for form-process linkages. Environmental Management, 57(4), 929-942.

967 Burnett KM, Reeves GH, Miller DJ, Clarke S, Vance-Borland K, and Christiansen K.
968 2007. Distribution Of Salmon-Habitat Potential Relative To Landscape
969 Characteristics And Implications For Conservation. Ecological Applications
970 17:66–80.http://dx.doi.org/10.1890/10510761(2007)017[0066:DOSPRT]2.0.CO;2

971 Caamaño D, Goodwin P, Buffington JM. 2009. Unifying criterion for the velocity reversal
972 hypothesis in gravel-bed rivers. Journal of Hydraulic Engineering 135: 66–70.

973 Carbonneau P, Fonstad MA, Marcus WA, Dugdale SJ. 2012. Making riverscapes real.
974 Geomorphology. 137:74-86. DOI: 10.1016/j.geomorph.2010.09.030

975 Carley JK, Pasternack GB, Wyrick JR, Barker JR, Bratovich PM., Massa D, Reedy G, ,
976 Johnson TR. 2012. Significant decadal channel change 58–67years post-dam
977 accounting for uncertainty in topographic change detection between contour
978 maps and point cloud models. Geomorphology 179: 71-88. DOI:
979 10.1016/j.geomorph.2012.08.001

980 Carling PA, Orr HG. 2000. Morphology of riffle-pool sequences in the River Severn,
981 England. Earth Surface Processes and Landforms 2 25: 369–384. DOI:
982 10.1002/(SICI)1096-9837(200004)25:4<369::AID-ESP60>3.0.CO;2-M

983 Carter G, Knapp C, Nuttall A. 1973. Estimation of the magnitude-squared coherence
984 function via overlapped fast Fourier transform processing. IEEE Transactions on
985 Audio and Electroacoustics 21: 337 – 344. DOI: 10.1109/TAU.1973.1162496

986 Cherkauer DS. 1973. Minimization of power expenditure in a riffle-pool alluvial channel.
987 Water Resources Research 9: 1613–1628.

988 Cienciala P, Pasternack, GB. in press. Floodplain Inundation Response to Climate,
989 Valley Form, and Flow Regulation on a Gravel-Bed River in a Mediterranean-
990 Climate Region. Geomorphology.

991 . Church, M, 2006. Multiple scales in rivers, In: Helmut Habersack, Hervé Piégay and
992 Massimo Rinaldi, Editor(s), Developments in Earth Surface Processes, Elsevier,
993 2007, Volume 11, Pages 3-28, ISSN 0928-2025, ISBN 9780444528612,
994 http://dx.doi.org/10.1016/S0928-2025(07)11111-
995 1.(http://www.sciencedirect.com/science/article/pii/S0928202507111111)

996 Colombini M, Seminara G, Tubino M. 1987. Finite-amplitude alternate bars. Journal of
997 Fluid Mechanics 181: 213-232. DOI: 10.1017/S0022112087002064

Cox N, J. 1983. On the estimation of spatial autocorrelation in geomorphology. Earth Surface Processes and Landforms 8: 89–93. DOI: 10.1002/esp.3290080109

Davis, W.M., 1909. The Geographical Cycle, Chapter 13, Geographical Essays. Ginn and Co., New York.

DeAlmeida GAM, Rodriguez JF. 2012. Spontaneous formation and degradation of pool-riffle morphology and sediment sorting using a simple fractional transport model. Geophysical Research Letters 39, L06407, doi:10.1029/2012GL051059.

Dolan R, Howard A, Trimble D. 1978. Structural control of the rapids and pools of the Colorado River in the Grand Canyon. Science 10: 629-631. DOI: 10.1126/science.202.4368.629

Doyle MW, Shields D, Boyd KF, Skidmore PB, Dominick D. 2007. Channel-Forming Discharge Selection in River Restoration Design. Journal of Hydraulic Engineering 133(7):831-837.

Escobar-Arias MI, Pasternack G.B. 2011. Differences in River Ecological Functions Due to Rapid Channel Alteration Processes in Two California Rivers Using the Functional Flows Model, Part 2- Model Applications. River Research and Applications 27, 1–22, doi: 10.1002/rra.1335.

Frissell CA, Liss WJ, Warren CE, Hurley MD. 1986. A hierarchical framework for stream habitat classification: Viewing streams in a watershed context. Environmental Management 10(2): 199-214.

Gangodagamage, C, Barnes, E, Foufoula Georgiou, E. 2007. Scaling in river corridor widths depicts organization in valley morphology, Geomorphology, 91, 198–215, doi:10.1016/j.geomorph.2007.04.014.

Gessese AF, Sellier M, Van Houten E, Smart, G. 2011. Reconstruction of river bed topography from free surface data using a direct numerical approach in one-dimensional shallow water flow. Inverse Problems 27.

Gilbert GK, 1917. Hydraulic-mining debris in the Sierra Nevada. United States Geological Survey Professional Paper 105.

Ghoshal S, James LA, Singer MB, Aalto R. 2010. Channel and Floodplain Change Analysis over a 100-Year Period: Lower Yuba River, California. Remote Sensing, 2(7): 1797.

Guinn JM. 1890. Exceptional years: a history of California floods and drought. Historical Society of Southern California 1 (5): 33-39.

1031 Harman C, Stewardson M, DeRose R. 2008. Variability and uncertainty in reach
1032 bankfull hydraulic geometry. Journal of Hydrology 351(1-2):13-25, ISSN 0022-
1033 1694, http://dx.doi.org/10.1016/j.jhydrol.2007.11.015.

1034 Harrison LR, Keller EA. 2007. Modeling forced pool–riffle hydraulics in a boulder-bed
1035 stream, southern California. Geomorphology 83: 232–248. DOI:
1036 10.1016/j.geomorph.2006.02.024

1037 Hernandez G. 1999. Time series, periodograms, and significance, J. Geophys. Res.,
1038 104(A5), 10355–10368, doi:10.1029/1999JA900026.

1039 Hey RD, Thorne CR. 1986. Stable channels with mobile gravel beds. Journal of
1040 Hydraulic Engineering 112: 671–689.

1041 Huang HQ, Chang HH, Nanson GC.2004. Minimum energy as the general form of
1042 critical flow and maximum flow efficiency and for explaining variations in river
1043 channel pattern, Water Resour. Res., 40, W04502, doi:10.1029/2003WR002539.

1044 Huang HQ, Deng C, Nanson GC, Fan B, Liu X, Liu T, Ma Y. 2014. A test of equilibrium
1045 theory and a demonstration of its practical application for predicting the
1046 morphodynamics of the Yangtze River. Earth Surf. Process. Landforms, 39: 669–
1047 675.

1048 Jackson JR, Pasternack GB, Wyrick JR. 2013. Substrate of the Lower Yuba River.
1049 Prepared for the Yuba Accord River Management Team. University of California,
1050 Davis, CA, 61pp.

1051 James LA, Singer MB, Ghoshal S. 2009. Historical channel changes in the lower Yuba
1052 and Feather Rivers, California: Long-term effects of contrasting river-
1053 management strategies. Geological Society of America Special Papers 451:57-
1054 81. DOI: 10.1130/2009.2451(04

1055 Keller E. 1971. Areal Sorting of Bed-Load Material: The Hypothesis of Velocity
1056 Reversal. Geological Society of America Bulletin 82: 753-756.

1057 Keller EA, Melhorn WN. 1978. Rhythmic spacing and origin of pools and riffles: GSA
1058 Bulletin 89: 723-730. DOI: 10.1130/0016-7606(1978)89<723:RSAOOP>2.0.CO;2

1059 Knighton A. 1983. Models of stream bed topography at the reach scale. Journal of
1060 Hydrology 60.

1061 Lisle, T 1979. A Sorting Mechanism For A Riffle-Pool Sequence. Geological Society of
1062 America Bulletin, Part 11. 90: 1142-1157.

1063 Leopold LB, Maddock T. 1953. The Hydraulic Geometry of Stream Channels and Some
1064 Physiographic Implications. Geological Survey Professional Paper 252, United
1065 States Geological Survey, Washington, D.C.

1066 Leopold, LB and Langbein, WB. 1962. The Concept of Entropy in Landscape Evolution,
1067 U.S. Geological Survey Professional Paper 500-A, 20p.

1068 MacWilliams, ML, Jr, Wheaton, JM, Pasternack, GB, Street, RL, Kitanidis, PK. 2006.
1069 Flow convergence routing hypothesis for pool–riffle maintenance in alluvial rivers.
1070 Water Resources Research 42, W10427. doi:10.1029/2005WR004391.

1071 Madej MA. 2001. Development of channel organization and roughness following
1072 sediment pulses in single-thread, gravel bed rivers. Water Resources Research
1073 37: 2259-2272. DOI: 10.1029/2001WR000229

1074 Magirl CS, Webb RH, Griffiths PG. 2005. Changes in the water surface profile of the
1075 Colorado River in Grand Canyon, Arizona, between 1923 and 2000, Water
1076 Resour. Res., 41, W05021, doi:10.1029/2003WR002519.

1077 MacVicar BJ, Rennie CD. 2012. Flow and turbulence redistribution in a straight artificial
1078 pool. Water Resources Research 48, W02503, doi:10.1029/2010WR009374

1079 Marquis GA, Roy AG. 2011. Bridging the gap between turbulence and larger scales of
1080 flow motions in rivers. Earth Surface Processes and Landforms 36: 563–568.
1081 doi:10.1002/esp.2131

1082 McKean JA, Isaac DJ, Wright CW. 2008. Geomorphic controls on salmon nesting
1083 patterns described by a new, narrow-beam terrestrial–aquatic lidar. Frontiers in
1084 Ecology and the Environment 6: 125-130. DOI: 10.1890/070109

1085 McKean J, Nagel D, Tonina D, Bailey P, Wright CW, Bohn,C, Nayegandhi A, 2009.
1086 Remote sensing of channels and riparian zones with a narrow-beam aquatic-
1087 terrestrial lidar. Remote Sensing, 1, 1065-1096; doi:10.3390/rs1041065.

1088 Melton MA. 1962. Methods for measuring the effect of environmental factors on channel
1089 properties. Journal of Geophysical Research 67: 1485-1490. DOI:
1090 10.1029/JZ067i004p01485

1091 Milan DJ, Heritage GL, Large ARG, Charlton ME. 2001. Stage dependent variability in
1092 tractive force distribution through a riffle-pool sequence. Catena 44: 85-109.

1093 Milne JA. 1982. Bed-material size and the riffle-pool sequence. Sedimentology 29: 267-
1094 278. DOI: 10.1111/j.1365-3091.1982.tb01723.x

1095 Nelson PA, Brew AK, Morgan, JA. 2015. Morphodynamic response of a variable-width
1096 channel to changes in sediment supply. Water Resources Research 51: 5717–
1097 5734, doi:10.1002/2014WR016806.

1098 Newland DE. 1993. An introduction to random vibrations, spectral and wavelet analysis.
1099 Dover Publications.

1100 Nickelson TA, Rodgers J, Steven L. Johnson, Mario F. Solazzi. 1992. Seasonal
1101 Changes in Habitat Use by Juvenile Coho Salmon (Oncorhynchus kisutch) in
1102 Oregon Coastal Streams. Canadian Journal of Fisheries and Aquatic Sciences,
1103 1992, 49:783-789, 10.1139/f92-088

1104 Nolan KM, Lisle TE, Kelsey HM. 1987. Bankfull discharge and sediment transport in
1105 northwestern California. In: R. Beschta, T. Blinn, G. E. Grant, F. J. Swanson, and
1106 G. G. Ice (ed.), Erosion and Sedimentation in the Pacific Rim (Proceedings of the
1107 Corvallis Symposium, August 1987). International Association of Hydrological
1108 Sciences Pub. No. 165, p. 439-449.

1109 Parker G., Toro-Escobar CM, Ramey M, Beck S, 2003. The effect of floodwater
1110 extraction on the morphology of mountain streams. Journal of Hydraulic
1111 Engineering, 129(11): 885-895.

1112 Pasternack GB, Tu D, Wyrick JR. 2014. Chinook adult spawning physical habitat of the
1113 lower Yuba River. Prepared for the Yuba Accord River Management Team.
1114 University of California, Davis, CA, 154pp.

1115 Pasternack GB, Wyrick JR. in press. Flood-driven topographic changes in a gravel-
1116 cobble river over segment, reach, and unit scales. Earth Surface Processes and
1117 Landforms

1118 Park CC. 1977. World-wide variations in hydraulic geometry exponents of stream
1119 channels: An analysis and some observations, Journal of Hydrology 33(1): 133-
1120 146, ISSN 0022-1694, http://dx.doi.org/10.1016/0022-1694(77)90103-2.

1121 Phillips PJ, Harlin JM.1984. Spatial dependency of hydraulic geometry exponents in a
1122 subalpine stream, Journal of Hydrology 71(3): 277-283. ISSN 0022-1694,
1123 http://dx.doi.org/10.1016/0022-1694(84)90101-X.

1124 Pike RJ, Evans I, Hengl T. 2008. Geomorphometry: A Brief Guide. In: Geomorphometry
1125 - Concepts, Software, Applications, Hengl, T. and Hannes I. Reuter (eds.), Series
1126 Developments in Soil Science vol. 33, Elsevier, pp. 3-33, ISBN 978-0-12-374345-
1127 9

Rayburg SC, Neave M. 2008. Assessing morphologic complexity and diversity in river systems using three-dimensional asymmetry indices for bed elements, bedforms and bar units. River Research and Applications 24: 1343–1361. DOI: 10.1002/rra.1096

Rendell H, Alexander D. 1979. Note on some spatial and temporal variations in ephemeral channel form. Geological Society of America Bulletin 9: 761-772. DOI: 10.1130/0016-7606(1979)90<761:NOSSAT>2.0.CO;2

Repetto R, Tubino M, 2001. Topographic Expressions of Bars in Channels with Variable Width. Phys. Chem. Earth (B), Vol. 26:71-76.

Richards KS. 1976a. The morphology of riffle-pool sequences. Earth Surface Processes 1: 71-88. DOI: 10.1002/esp.3290010108

Richards KS. 1976b. Channel width and the riffle-pool sequence. Geological Society of America Bulletin 87: 883-890.

Richards KS. 1979. Stochastic processes in one dimension: An introduction. Concepts and Techniques In Modern Geography No. 23. 30 pages.

Richter BD, Braun DP, Mendelson MA, Master LL. 1997. Threats to Imperiled Freshwater Fauna. Conservation Biology 11: 1081–1093.

Rosgen D, 1996. Applied River Morphology (Wildland Hydrology, Pagosa Springs, Colorado). Wildland Hydrology, Pagosa Springs, CO.

Salas JD. 1980. Applied modeling of hydrologic time series. Applied modeling of hydrologic time series. Water Resources Publications. Littleton, Colorado.

Sawyer, AM, Pasternack GB, Moir HJ, Fulton AA. 2010. Riffle-pool maintenance and flow convergence routing confirmed on a large gravel bed river. Geomorphology, 114: 143-160

Schumm SA. 1971. Fluvial geomorphology: channel adjustment and river metamorphosis. In: Shen, H.W. (Ed.), River Mechanics. H.W. Shen, Fort Collins, CO, pp. 5-1–5-22.

Shields D, Copeland R., Klingeman P, Doyle M, and Simon A. 2003. Design for Stream Restoration. Journal of Hydraulic Engineering 10.1061/(ASCE)0733-9429(2003)129:8(575), 575-584.

Shumway RH, Stoffer DS. 2010. Time series analysis and its applications: with R examples. Time series analysis and its applications: with R examples. 505 pages. Springer US.

1161 Simon AM, Doyle M, Kondolf M, Shields FD, Rhoads B, and McPhillips M. 2007. Critical
1162 Evaluation of How the Rosgen Classification and Associated ‘‘Natural Channel
1163 Design’’ Methods Fail to Integrate and Quantify Fluvial Processes and Channel
1164 Response. Journal of the American Water Resources Association 43(5):1117-
1165 1131. DOI: 10.1111 / j.1752-1688.2007.00091.x

1166 Strom MA, Pasternack GB, Wyrick JR. 2016. Reenvisioning velocity reversal as a
1167 diversity of hydraulic patch behaviors. Hydrologic Processes, doi:
1168 10.1002/hyp.10797.

1169 Surian N, Mao L, Giacomin M, and Ziliani L. 2009. Morphological effects of different
1170 channel-forming discharges in a gravel-bed river. Earth Surface Processes and
1171 Landforms 34: 1093–1107. doi:10.1002/esp.1798

1172 Thomson JR, Taylor MP, Fryirs KA, Brierley GJ. 2001. A geomorphological framework
1173 for river characterization and habitat assessment. Aquatic Conservation-Marine
1174 and Freshwater Ecosystems, 11(5), 373-389.

1175 Thompson DM. 2010. The velocity-reversal hypothesis revisited. Progress in Physical
1176 Geography 35: 123–132. DOI: 10.1177/0309133310369921

1177 Thornbury WD. 1954. Principles of geomorphology. John Wiley, New York.

1178 Trauth MH, Gebbers R, Marwan N, Sillmann E. 2006. MATLAB recipes for earth
1179 sciences. Springer

1180 Wolman MG, Gerson R. 1978. Relative Scales of Time and Effectiveness of Climate in
1181 Watershed Geomorphology. Earth Surface Processes and Landforms 3(2): 189-
1182 208.

1183 White JQ, Pasternack GB, Moir HJ. 2010. Valley width variation influences riffle–pool
1184 location and persistence on a rapidly incising gravel-bed river. Geomorphology
1185 121: 206–221. DOI: 10.1016/j.geomorph.2010.04.012

1186 Wilkinson SN, Keller RJ, Rutherfurd ID. 2004. Phase-shifts in shear stress as an
1187 explanation for the maintenance of pool–riffle sequences. Earth Surface
1188 Processes and Landforms 29: 737–753. DOI: 10.1002/esp.1066

1189 Williams GP. 1978. Bank-full discharge of rivers, Water Resources Research 14:1141–
1190 1154. doi:10.1029/WR014i006p01141.

1191 Wohl EE, Thompson DM, Miller AJ. 1999. Canyons with undulating walls, Geological
1192 Society of America Bulletin 111, 949–959.

Wyrick JR, Pasternack GB. 2012. Landforms of the lower Yuba River. University of California, Davis.

Wyrick JR, Pasternack GB. 2014. Geospatial organization of fluvial landforms in a gravel–cobble river: Beyond the riffle–pool couplet. Geomorphology 213: 48-65. DOI: 10.1016/j.geomorph.2013.12.040

Wyrick JR, Pasternack GB. 2015. Revealing the natural complexity of topographic change processes through repeat surveys and decision-tree classification. Earth Surface Processes and Landforms, doi: 10.1002/esp.3854.

Yalin, MS. 1977. Mechanics of sediment transport. Elsevier

Yang CT. 1971. Potential Energy and Stream Morphology. Water Resources Research 7. DOI: 10.1029/WR007i002p00311

Yu B, Wolman MG. 1987. Some dynamic aspects of river geometry, Water Resources Research 23(3): 501–509. doi:10.1029/WR023i003p00501.

11. List of Figures

Figure 1. Regional and vicinity map of the lower Yuba River (A) and extent of study segment showing inundation extents predicted by the 2D model (B).

Figure 2. Raw bed profile (A) and flow width (B) series for 283.2 m^3/s. After detrending and standardizing, values of Z (black line in C) and W (blue line in C) are multiplied together to compute $C(Z,W^j)$ (red line in C). The whole series of $C(Z,W^j)$ is the GCS

Figure 3. Conceptual key for interpreting $C(Z,W^j)$ geomorphic covariance structures (A). For quadrant 1 Z and W^j are both relatively high, so that implies wide and shallow areas associated with deposition. Conversely, in quadrant 2 Z is relatively low, but and W^j is relatively high, which implies deep and wide cross areas, which implies that these areas may have been scoured at larger flows. In quadrant 3 Z and W^j are both

relatively low, so that implies narrow and deep areas associated with erosion. Finally, in quadrant 4 Z is relatively high and W^j is relatively low, so that implies narrow and topographically high areas. Prototypical channels and GCS with positive (B), and negative (C) $C(Z, W^j)$ colored according to (A).

Figure 4. Example section in the middle of the study area showing inundation extents (A). Below are plots of minimum bed elevation (B), flow widths for 8.50 m^3/s, 283.2 m^3/s, and 3,126 m^3/s (C), and $C(Z, W^j)$for the same flows. The aerial image is for a flow of 21.29 m^3/s on 9/28/2006.

Figure 5. Example section at the lower extent of the study area showing inundation extents (A). Below are plots of minimum bed elevation (B), flow widths for 8.50 m^3/s, 283.2 m^3/s, and 3,126 m^3/s (C), and $C(Z, W^j)$for the same flows. The aerial image is for a flow of 21.29 m^3/s on 9/28/2006.

Figure 6. Histogram of $C(Z, W^j)$ classified by positive and negative values as well as > and < 1 (A). Also shown is a histogram classified by quadrant (B). Both illustrate an overall tendency for $C(Z, W^j) > 0$ with increasing discharge and also illustrating an increasing tendency for positive values of $C(Z, W^j) > 1$ up until 283.2 m^3/s after which it declines. Colors represent bin centered values.

Figure 7. Pearson's correlation coefficient for Z and W^j between each flow.

Figure 8. Pearson's correlation coefficient for sequential pairs of flow dependent wetted width series.

Figure 9. Autocorrelation (A) and PSD (B) of $C(Z, W^j)$ with increasing flow. For the ACF plot (A), only values exceeding white noise at the 95% level are shown and the red countor demarcates the 95% level for an AR1 process(red noise). For the PSD plot (B) only values exceeding white noise at the 95% level are shown.

Table 1. Flows analyzed and their approximate annual recurrence intervals.

Table 2. Linear trend models and R^2 for Z and W^j used in detrending each series.

Table 3. Mann Whitney U-test p values amongst all combinations of Z and W^j at the 95% level.

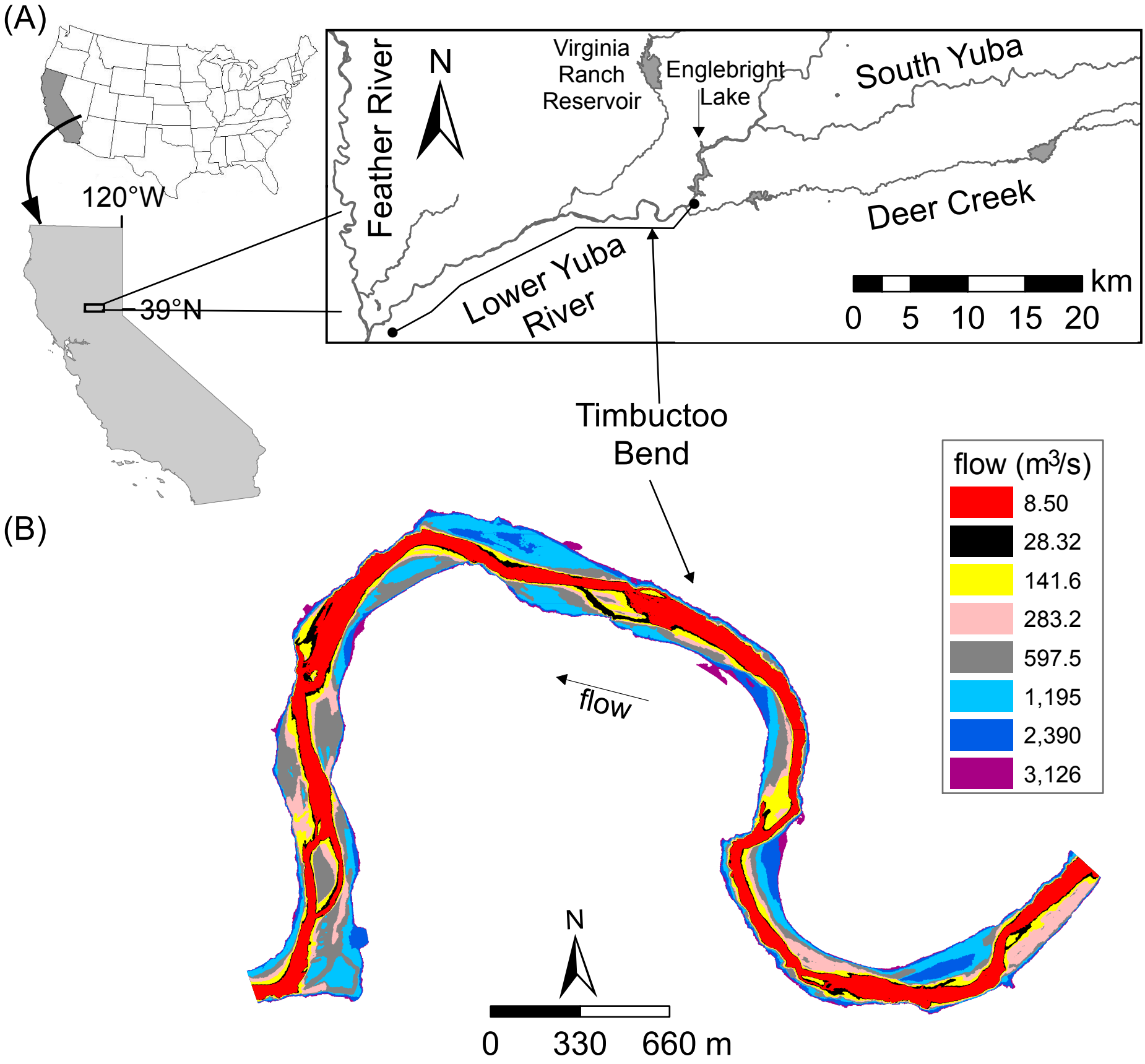
(A)
120°W
39°N
Feather River
N
Virginia
Ranch
Reservoir
Englebright
Lake
South Yuba
Deer Creek
Lower Yuba
River
km
0 5 10 15 20
Timbuctoo
Bend
(B)
flow (m3/s)
8.50
28.32
141.6
283.2
597.5
1,195
2,390
3,126
flow
N
0 330 660 m

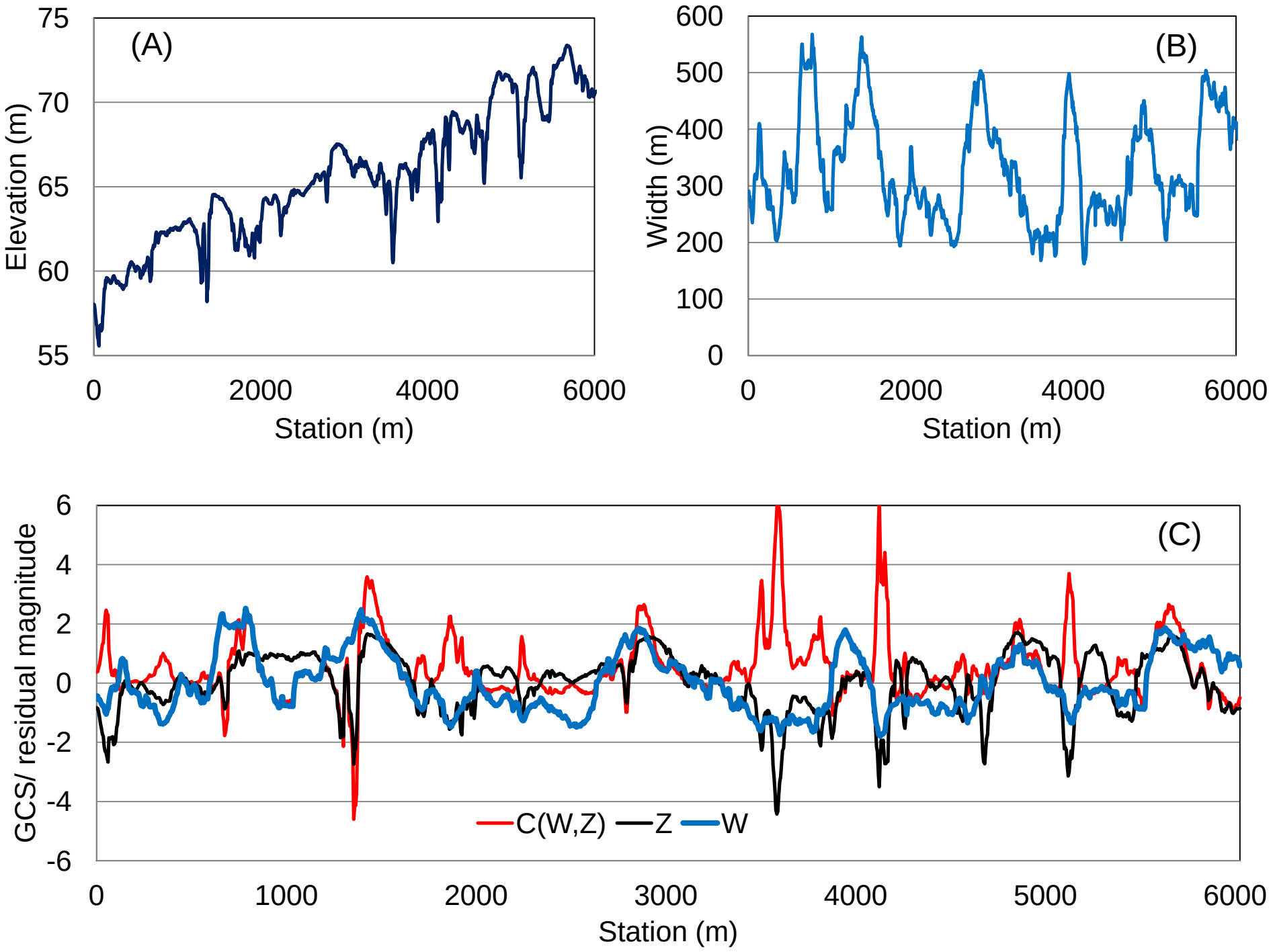
(A)
Elevation (m)
75
70
65
60
55
0
2000
4000
6000
Station (m)
(B)
Width (m)
600
500
400
300
200
100
0
0
2000
4000
6000
Station (m)
(C)
GCS/ residual magnitude
6
4
2
0
-2
-4
-6
C(W,Z)
Z
W
0
1000
2000
3000
4000
5000
6000
Station (m)

(A)

Relative Bed Elevation

-Z +Z

Relative Width

+ W^j | - C(Z, W^j) | +C(Z, W^j)

- W^j | + C(Z, W^j) | - C(Z, W^j)

(B)

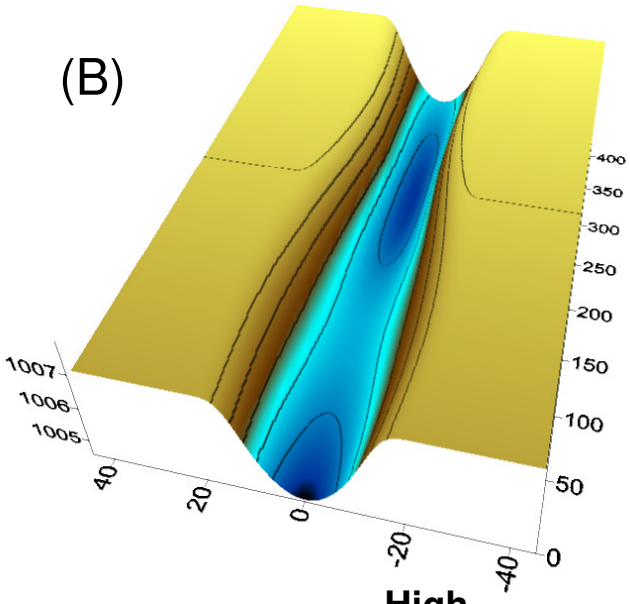

(C)

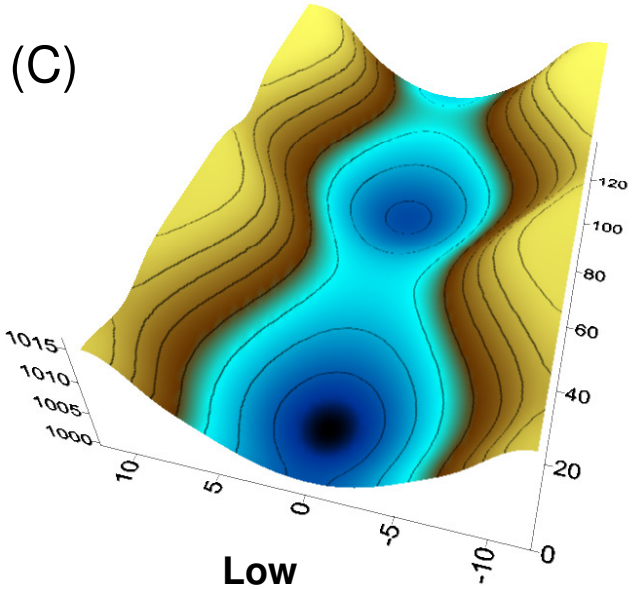

High

Low

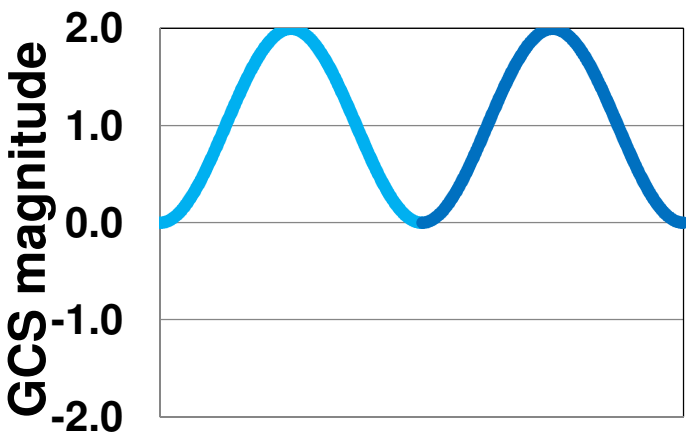

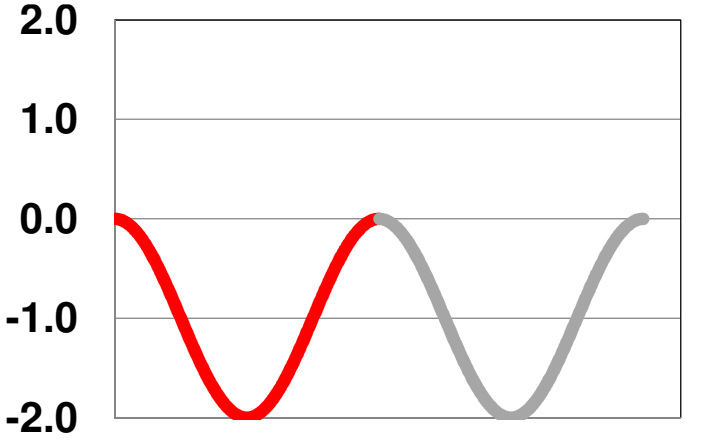

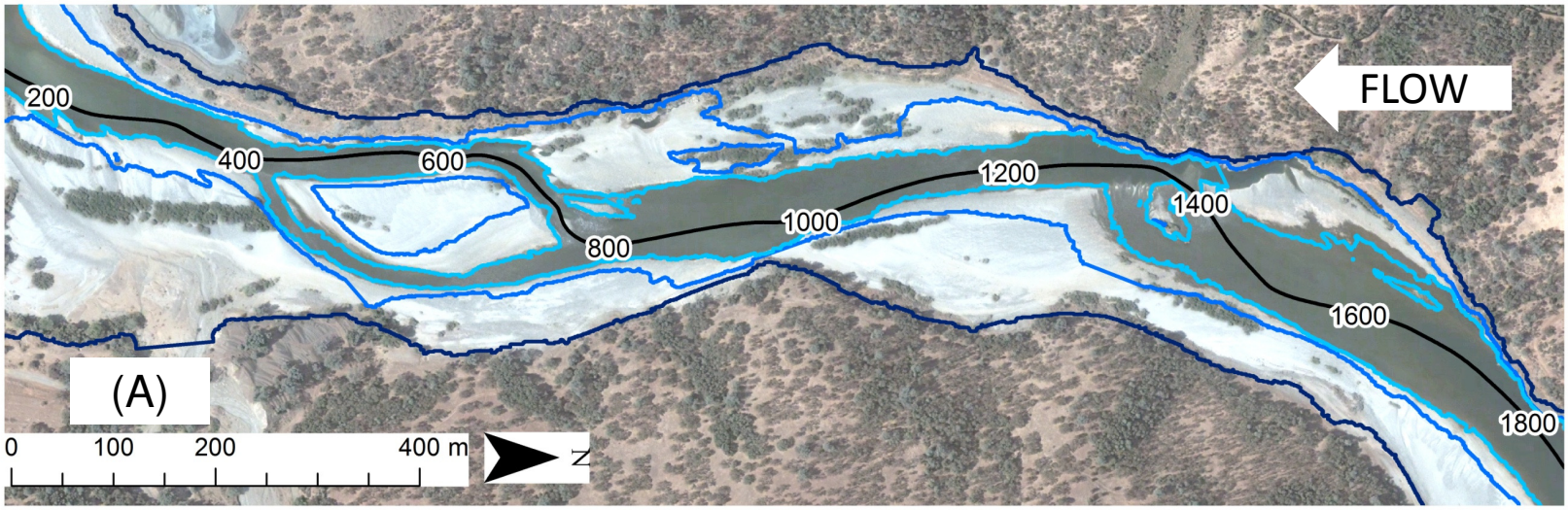
200
400
600
800
1000
1200
1400
1600
1800
FLOW
(A)
0
100
200
400 m
N

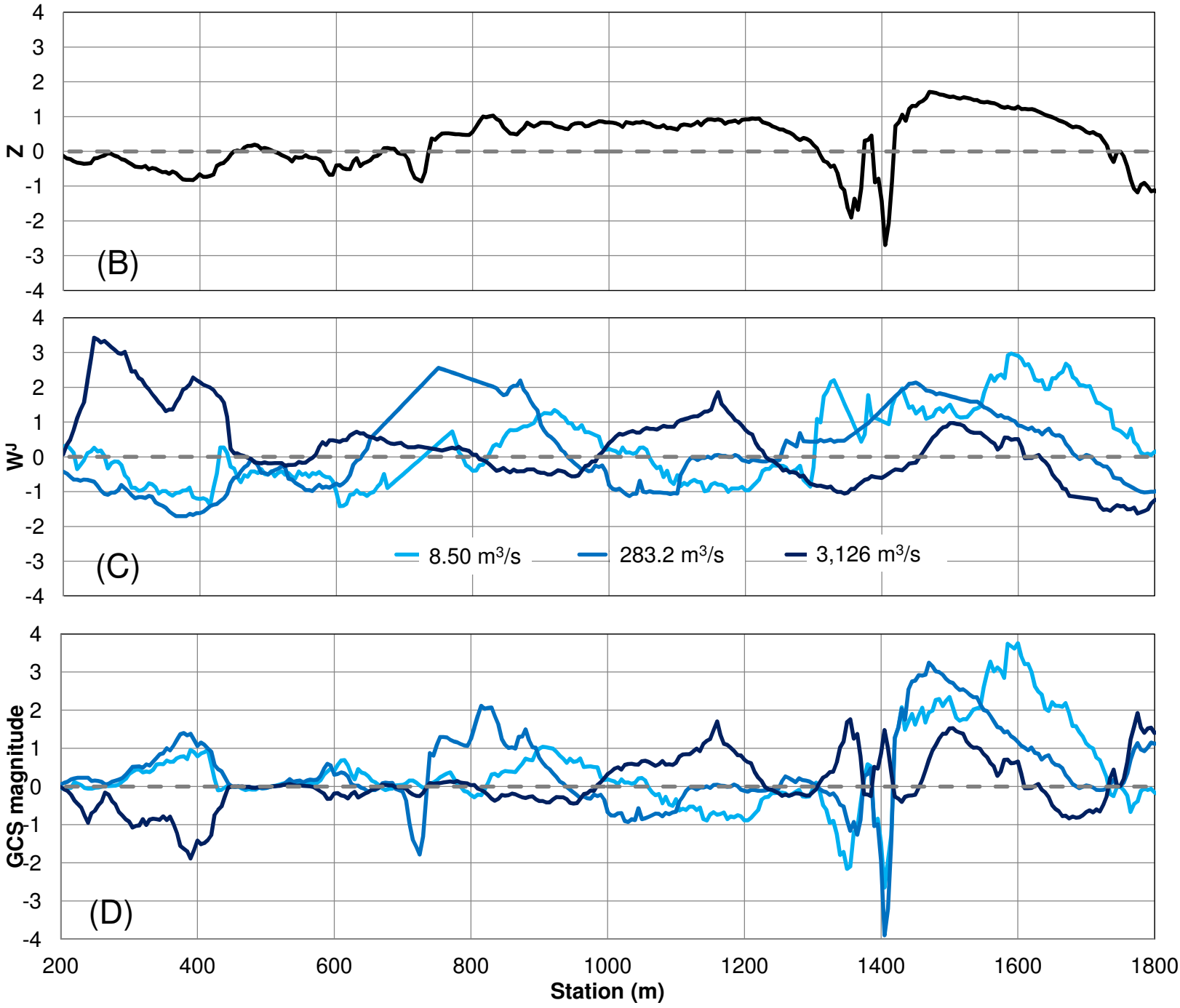
z
(B)
w^J
(C)
8.50 m³/s
283.2 m³/s
3,126 m³/s
GCS magnitude
(D)
Station (m)

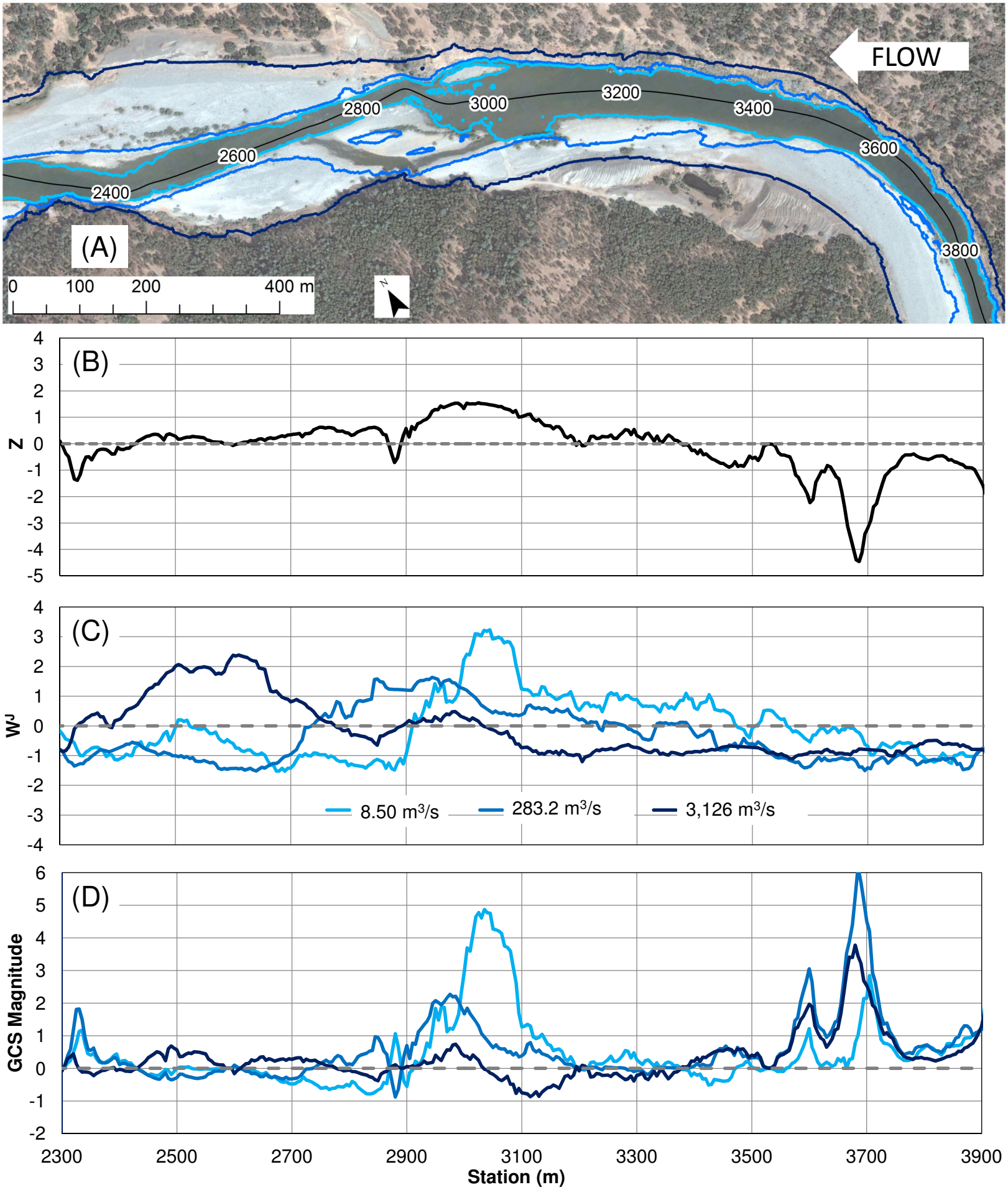
FLOW
2400
2600
2800
3000
3200
3400
3600
3800
(A)
0
100
200
400 m
N
(B)
Z
(C)
W^J
8.50 m³/s
283.2 m³/s
3,126 m³/s
(D)
GCS Magnitude
2300
2500
2700
2900
3100
3300
3500
3700
3900
Station (m)

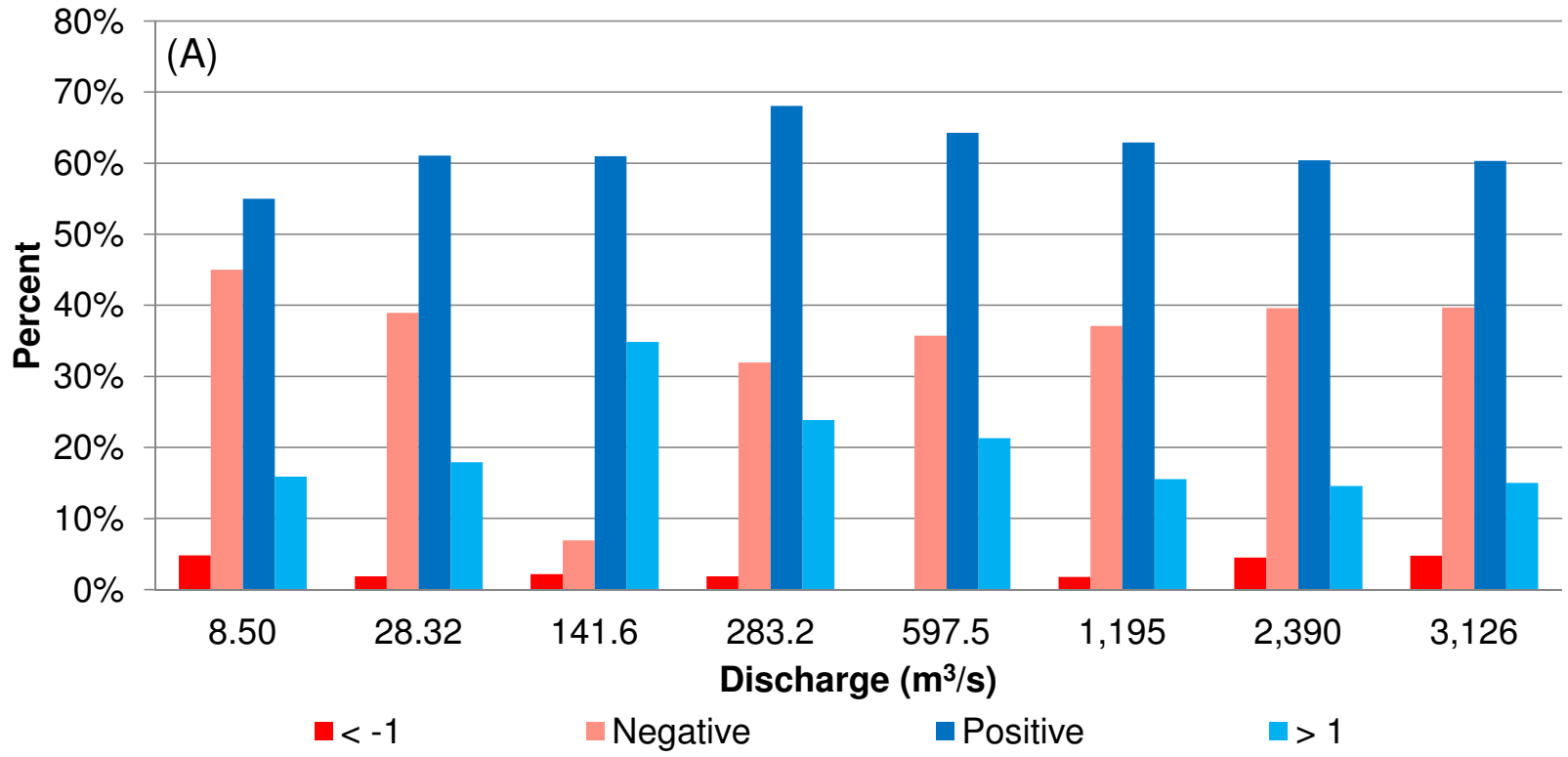
(A)
80%
70%
60%
50%
40%
30%
20%
10%
0%
Percent
8.50
28.32
141.6
283.2
597.5
1,195
2,390
3,126
Discharge (m3/s)
< -1
Negative
Positive
> 1

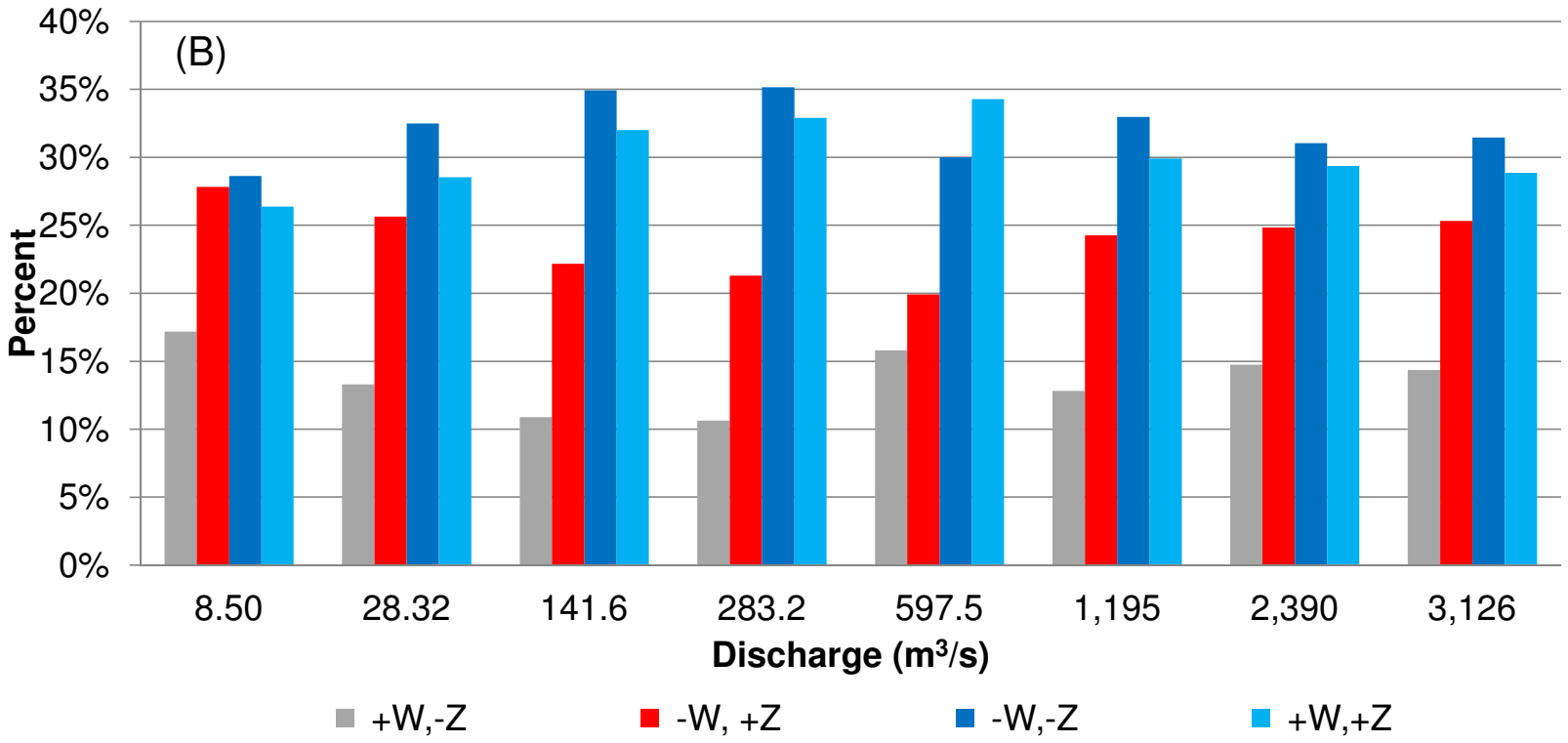
(B)
40%
35%
30%
25%
20%
15%
10%
5%
0%
Percent
8.50
28.32
141.6
283.2
597.5
1,195
2,390
3,126
Discharge (m3/s)
+W,-Z
-W, +Z
-W,-Z
+W,+Z

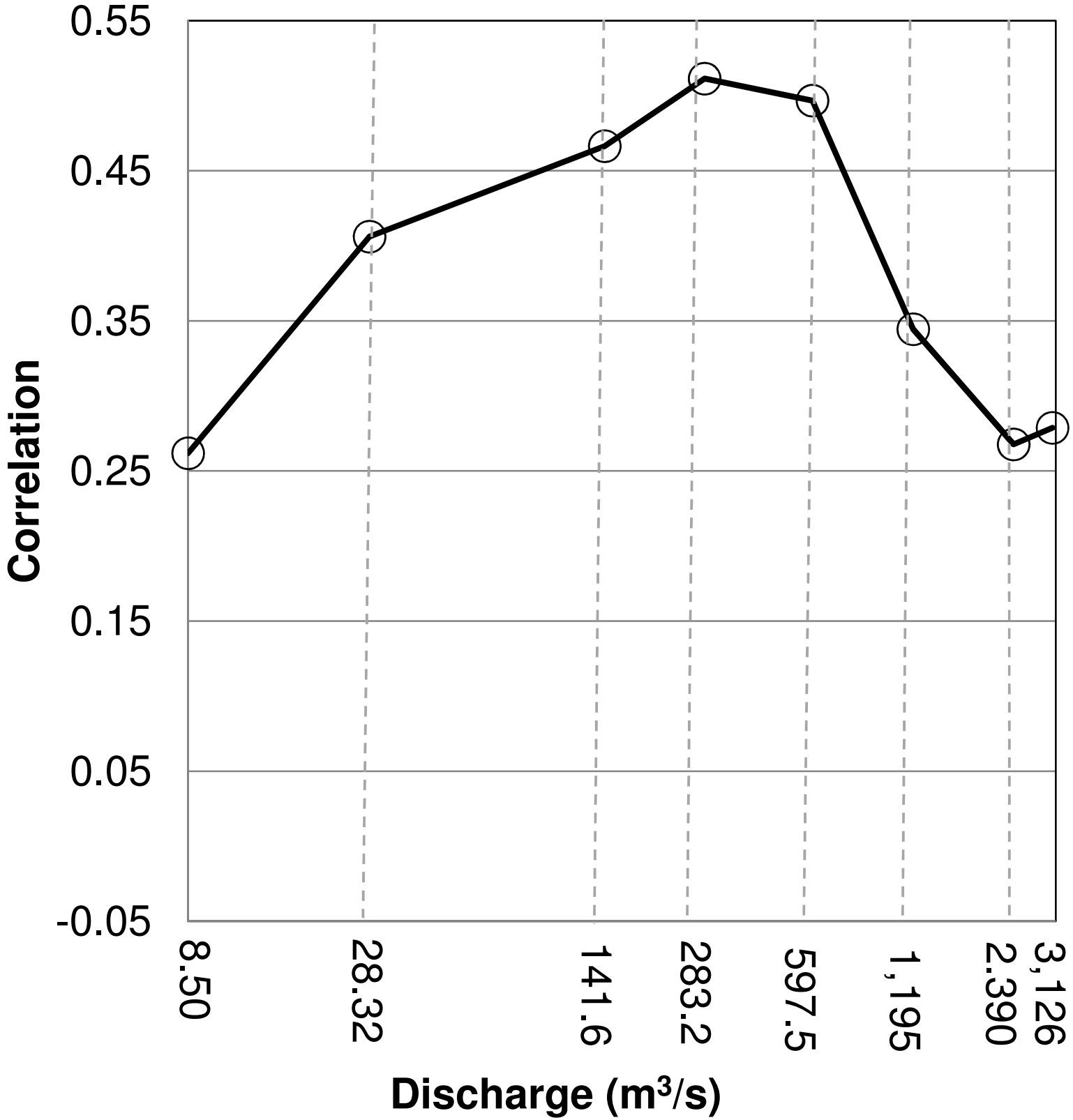
0.55
0.45
0.35
0.25
0.15
0.05
-0.05
Correlation
8.50
28.32
141.6
283.2
597.5
1,195
2,390
3,126
Discharge (m³/s)

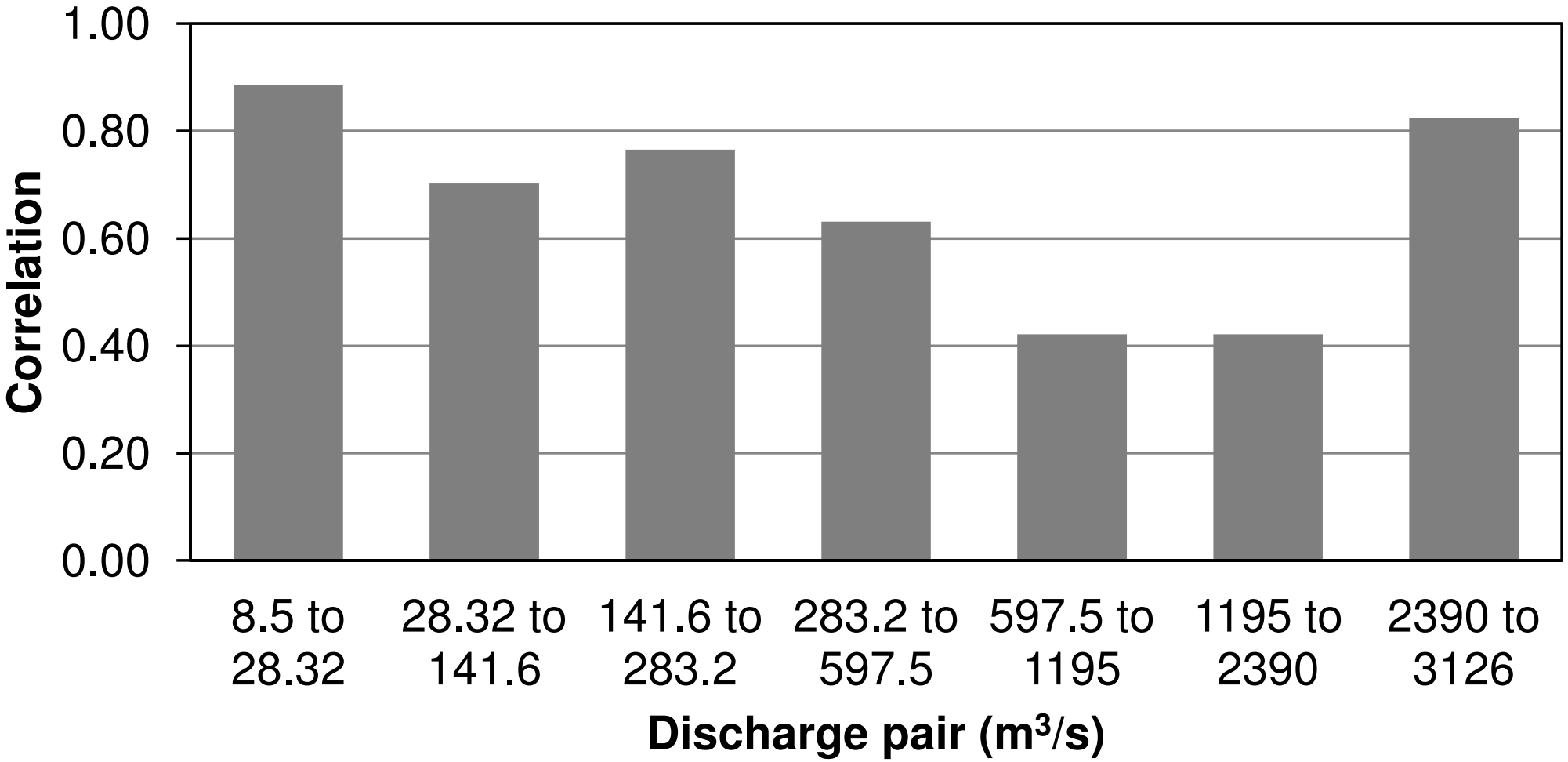
1.00
0.80
0.60
0.40
0.20
0.00
Correlation
8.5 to 28.32
28.32 to 141.6
141.6 to 283.2
283.2 to 597.5
597.5 to 1195
1195 to 2390
2390 to 3126
Discharge pair (m3/s)

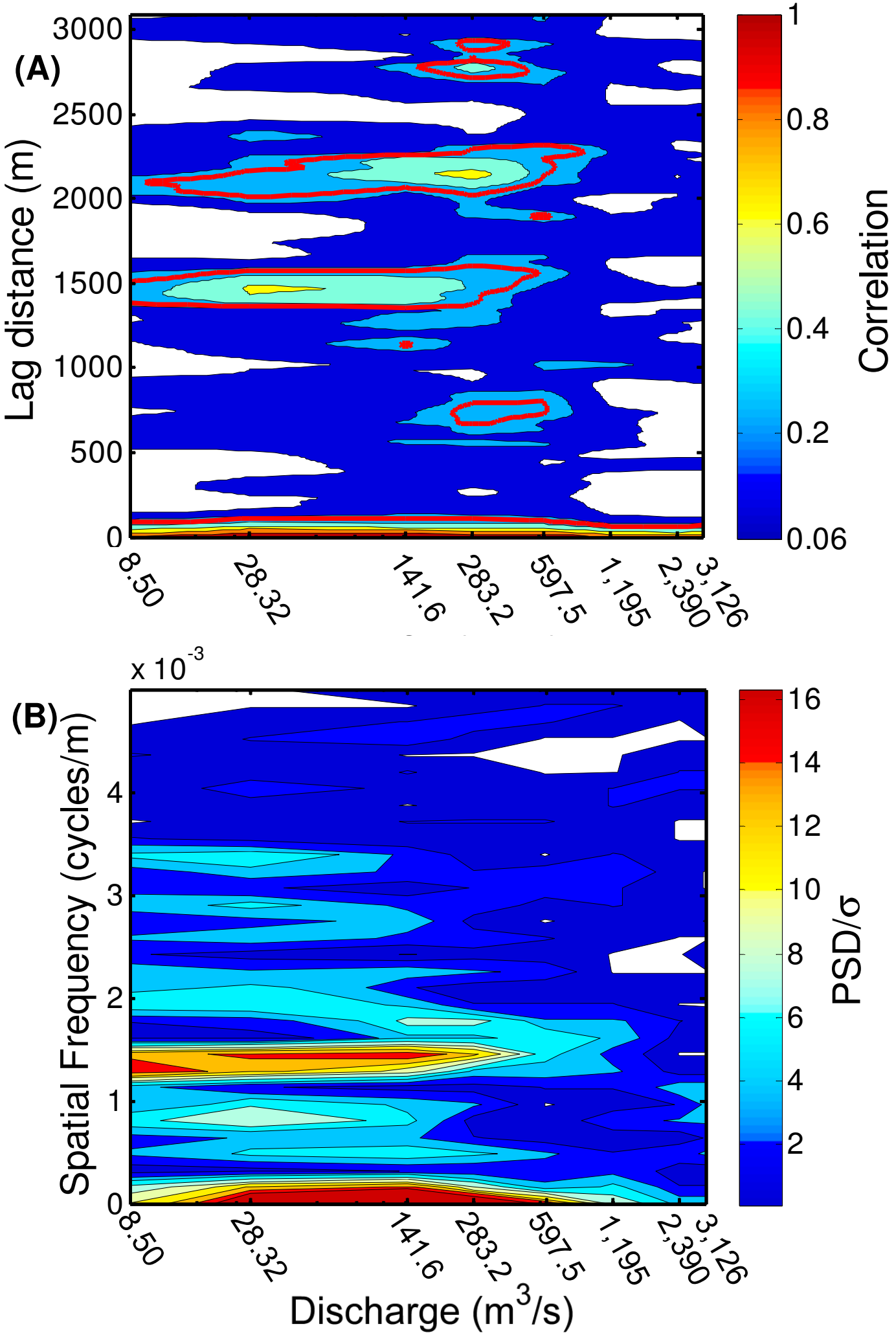
(A)
Lag distance (m)
3000
2500
2000
1500
1000
500
0
8.50
28.32
141.6
283.2
597.5
1,195
2,390
3,126
Correlation
1
0.8
0.6
0.4
0.2
0.06
(B)
x 10^-3
Spatial Frequency (cycles/m)
4
3
2
1
0
Discharge (m^3/s)
PSD/σ
16
14
12
10
8
6
4
2

Table 1. Flows analyzed and their approximate annual recurrence intervals

Q (m^3/s)	Approximate Recurrence Interval
8.50	1
28.32	1.03
141.6	1.2
283.2	1.5
597.5	2.5
1195	4.7
2390	12.7
3126	20

Table 2.Linear trend models and R2 for Z and W^j used in detrending each series

	Top width		Bed elevation	
Discharge (m^3/s)	Linear trend model	R^2	Linear trend model	R^2
8.50	y = -0.0016x + 193.03	0.0231	y = 0.002x + 194.2	0.8727
28.32	y = -0.0025x + 234.27	0.0429	y = 0.002x + 194.26	0.8713
141.6	y = -0.003x + 301.61	0.0423	y = 0.0021x + 194.04	0.8731
283.2	y = -0.0002x + 332.87	0.0002	y = 0.0021x + 194.23	0.8710
597.5	y = -0.0101x + 528.6	0.2286	y = 0.0021x + 194.16	0.8711
1,195	y = -0.0133x + 665.02	0.3037	y = 0.0021x + 194.29	0.8703
2,390	y = -0.012x + 710.57	0.2420	y = 0.0022x + 193.92	0.8736
3,126	y = -0.0121x + 733.12	0.2437	y = 0.0022x + 193.94	0.8733

Table 3.Mann Whitney U-test p values amongst all combinations of Z and W^j at the 95% level

	8.50	28.32	141.6	283.2	597.5	1,195	2,390	3,126
8.50		**0.0002**	**0.0000**	**0.0000**	**0.0000**	**0.0008**	**0.0498**	**0.0403**
28.32			**0.0126**	**0.0001**	**0.0262**	0.6152	0.0865	0.1009
141.6				0.125	0.7627	**0.0015**	**0.0000**	**0.0000**
283.2					0.0859	**0.0000**	**0.0000**	**0.0000**
597.5						**0.0033**	**0.0000**	**0.0001**
1195							0.2673	0.3129
2390								0.9487
3126								